Journal of Computational Physics 231 (2012) 1051–1079

Contents lists available at SciVerse ScienceDirect

Journal of Computational Physics

journal homepage: www.elsevier.com/locate/jcp

A review of Vlasov–Fokker–Planck numerical modeling of inertial confinement fusion plasma

A.G.R. Thomas [a,*], M. Tzoufras [b,1], A.P.L. Robinson [c], R.J. Kingham [d], C.P. Ridgers [d,2], M. Sherlock [d], A.R. Bell [b,c]

[a] Department of Nuclear Engineering and Radiological Sciences, University of Michigan, Ann Arbor, MI 48109, USA
[b] Clarendon Laboratory, University of Oxford, Parks Road, Oxford OX1 3PU, UK
[c] Central Laser Facility, STFC Rutherford-Appleton Laboratory, Chilton, Didcot, Oxfordshire OX11 0QX, UK
[d] The Blackett Laboratory, Imperial College London, London SW7 2AZ, UK

ARTICLE INFO

Article history:
Available online 5 October 2011

Keywords:
Computational
Vlasov
Fokker–Planck
Laser
Plasma
Inertial confinement fusion
Fast electron transport
Magnetic field

ABSTRACT

The interaction of intense lasers with solid matter generates a hot plasma state that is well described by the Vlasov–Fokker–Planck equation. Accurate and efficient modeling of the physics in these scenarios is highly pertinent, because it relates to experimental campaigns to produce energy by inertial confinement fusion on facilities such as the National Ignition Facility. Calculations involving the Vlasov–Fokker–Planck equation are computationally intensive, but are crucial to proper understanding of a wide variety of physical effects and instabilities in inertial fusion plasmas. In this topical review, we will introduce the background physics related to Vlasov–Fokker–Planck simulation, and then proceed to describe results from numerical simulation of inertial fusion plasma in a pedagogical manner by discussing some key numerical algorithm developments that enabled the research to take place. A qualitative comparison of the techniques is also given.

1. Introduction

The recently operational *National Ignition Facility*[3] and the soon to be completed *Laser MegaJoule*[4] facilities are designed to produce conditions similar to the core of a star here on earth, for purposes of scientific interest, energy research and national security. In inertial confinement fusion [1,2], a fuel pellet filled with deuterium–tritium fuel mixture is compressed by pressure due to plasma ablating from the walls of the capsule encasing the fuel. The ablation is caused by radiation heating, which is either *direct*, by laser heating, or *indirect*, by X-rays generated by laser heating of a *hohlraum* — a hollow, cylindrical, high-*Z* metal cavity — or possibly by other radiation sources such as a *Z*-pinch. The compressed fuel reaches a temperature and density comparable to that in the core of a star, initiating fusion reactions that rapidly heat the fuel and cause thermonuclear burn. In the case of the National Ignition Facility, now embarking on the *National Ignition Campaign* of experiments [3,4], this ablation is due to X-ray heating from radiation of approximately 300 eV temperature produced by 1.8 MJ of laser energy heating the interior walls of the hohlraum [5–7] – the indirect drive scheme of inertial confinement fusion.

* Corresponding author.
E-mail address: agrt@umich.edu (A.G.R. Thomas).
[1] Present address: University of California, Los Angeles, CA 90095, USA.
[2] Present address: Clarendon Laboratory, University of Oxford, Parks Road, Oxford OX1 3PU, UK.
[3] lasers.llnl.gov.
[4] www-lmj.cea.fr/.

0021-9991/$ - see front matter © 2011 Elsevier Inc. All rights reserved.
doi:10.1016/j.jcp.2011.09.028

The extremely high energy-density throughout the target means that the matter is in a plasma state, but not a plasma where we can ignore collisions and assume a fully ionized collection of classical point particles [8,9]. Radiation may be significant in determining how the plasma behaves, and under such conditions the plasma may even be Fermi degenerate. An ideal classical plasma is described only by long range electromagnetic interactions of inertial point particles, where an individual charged particle encounters multiple simultaneous *small*-angle deflections, which effectively means that it experiences predominantly macroscopic, volume averaged fields in the plasma. Such a plasma is found in hot, tenuous and highly ionized material, such as the interstellar medium or tokamak plasma.

When a high-power laser interacts with a solid material, as it does in inertial confinement fusion, the plasma is very hot, but is also locally very dense, and so does not behave like an ideal classical plasma everywhere. Collisions, that is to say correlations between particles that correspond to microscopic field structures, are important. Since collisions act to push the momentum distribution function for the particles towards a Maxwell–Boltzmann (or Fermi–Dirac) distribution, it is common to describe the inertial fusion plasma using a fluid description (e.g. [10,11]), relying on the distribution function being everywhere in local equilibrium. However, this is also not an accurate description for all regions of the plasma, as nonthermal distributions naturally arise as a consequence of the velocity dependence of the effect of collisions, the high temperatures obtained and the small spatial scales associated with a laser spot.

Numerical modeling is a crucial part of understanding the physics of direct and indirect drive inertial confinement fusion plasma experiments. Even considering only the plasma physics, simulation is extremely challenging as many physical effects require a fully kinetic description, particularly when considering schemes intrinsically entailing nonthermal populations such as *fast ignition* [12] or *shock ignition* [13]. Compared with a hydrodynamic fluid technique a kinetic model is computationally intensive, as such a model not only contains spatial information but also momentum coordinates, and is therefore of high dimensionality and rich in information. To model plasma we not only need to model the motion of particles in macroscopic electromagnetic fields, but also the collisional relaxation due to two-body interactions, particularly because of the relatively long timescales involved in an inertial fusion plasma. A good description of these interactions is the Maxwell–Vlasov–Fokker–Planck system of equations.

There are several areas where Vlasov–Fokker–Planck numerical modeling has contributed to our understanding of inertial confinement fusion plasma. In particular, nonlocal thermal electron transport (Sections 4 and 7), magnetic field generation and dynamics (Section 5) and fast electron transport for fast ignition (Section 6) are problems that have required Vlasov–Fokker–Planck numerical modeling. In this review we will give an overview of the 30 years of Vlasov–Fokker–Planck numerical modeling of inertial confinement fusion plasma since the first study by Bell et al. [14]. The review starts by introducing some of the history and background physics related to Vlasov–Fokker–Planck simulation, and then proceeds to describe results from numerical simulation of inertial fusion plasma in a pedagogical manner by introducing some key numerical algorithm developments that enabled the research to take place. A qualitative comparison of the techniques is also given.

1.1. Inertial confinement fusion overview

Investigations into controlled thermonuclear fusion via inertial confinement began in the early 1960s following early developments in laser technology, with the invention of doped glass lasers giving this particular impetus. Early exploratory programmes in the US and USSR remained classified until the early 1970s, but in 1972 the seminal paper of Nuckolls et al. was published in which it was shown that the implosion of a shell directly-driven by laser irradiation could lead to a gain of about 30 with 60 kJ of laser energy [15].

These results led to sustained study of both direct and indirect drive inertial fusion in the US, starting with a series of small laser systems. The next developmental landmark was in 1978; the 10 kJ, 20 beam *Shiva* system based at the Lawrence Livermore National Laboratory [16]. The degree of compression that was obtained in these experiments was less than was hoped for, and it was found that the cause of this was the conversion of a substantial amount of laser energy into hot electrons, i.e. suprathermal electrons with mean free paths that are long compared to the target dimensions of significance. The typical hot electron energy is a function of the product of laser intensity with wavelength squared, $I\lambda^2$, so laser frequency doubling and tripling can substantially mitigate this problem. This led to an interest in developing shorter wavelength laser technology for direct-drive.

Hot electrons were not the only problem encountered in inertial confinement fusion research. It was also clear that irradiation uniformity and the Rayleigh–Taylor instability [17,18] were problems that needed to be solved. Both of these issues are much less problematic in the indirect drive approach than in the direct drive approach. This led to indirect drive being the focus of the next major laser system at the Lawrence Livermore National Laboratory; the *Nova* laser system [19]. *Nova* was a 10 beam facility that could deliver 40 kJ in 1 ns at a wavelength of 0.351 μm. Experiments on the *Nova* laser started in 1985, and these experiments resulted in considerable progress in the indirect drive approach.

Until the outcome of a review by the US National Academy of Sciences into the US inertial confinement fusion program in 1989–1990 [20,6], the success that was achieved on *Nova* was thought be leading to a "Laser Microfusion Facility" as a next step. This would have been based on a 5–10 MJ laser and would have aimed to achieve a gain of 100–200. The National Academy of Sciences review instead recommended that the next step be a somewhat smaller system that would still aim to demonstrate ignition, i.e. what is now known as the National Ignition Facility. The endorsement of the National Ignition Facility was contingent on outcome of a series of experiments on *Nova*. The results of these experiments indeed indicated that ignition could be reached on the proposed 1.8 MJ system. Construction of the National Ignition Facility took place from 1997 to

2009, and at the time of writing the National Ignition Campaign is well underway [4], with the results of early experiments suggesting that ignition conditions are being approached [7].

Although the development of indirect-drive inertial confinement fusion at the Lawrence Livermore National Laboratory has been a significant portion of inertial fusion research, a considerable amount of activity has taken place elsewhere. Direct-drive inertial confinement fusion based on central hot spot ignition has continued to be researched at both the Laboratory for Laser Energetics (using the OMEGA laser[5]) and the Naval Research Laboratory for example. In France, work has begun on the Laser MegaJoule, a comparable system to the National Ignition Facility. Since the late 1990s there has also been considerable interest in advanced inertial confinement fusion concepts, particularly the *fast ignition* concept proposed by Tabak et al. [12], and the *shock ignition* concept proposed by Betti et al. [13]. In Japan the GEKKO XII system at the Institute of Laser Engineering, Osaka has been upgraded for fast ignition research, a facility known as FIREX [21]. In Europe a large scale post-ignition research facility, the *HiPER* project, is under consideration,[6] along with a number of other laser systems. Preparation for these expensive large scale facilities requires extensive numerical modeling support.

2. Modeling hot dense plasma

2.1. Vlasov's plasma

It was Vlasov who first pointed out the unique behavior of plasma [8,9]. He argued that "*. . .for a system of charged particles the kinetic equation method which considers only binary interactions — interactions through collisions — is an approximation which is strictly speaking inadequate, so that in the theory of such systems an essential role must be played by the interaction forces, particularly at large distances and, hence, a system of charged particles is, in essence, not a gas but a distinctive system coupled by long-range forces*" [9]. His resulting formulation of the plasma interaction problem led to the famous Vlasov–Maxwell system of equations, which well describes a "classical" plasma under important constraints including the Debye–Hückel screening effect [22] and that long-range interaction timescales are much shorter than typical two-body interaction timescales. These long range electromagnetic interactions lead to collective effects, including plasma oscillations with characteristic angular frequency $\omega_p^2 = e^2 n_0/m_e\epsilon_0 + \sum_s q_s^2 n_0/m_s\epsilon_0 \simeq \omega_{pe}^2 = e^2 n_0/m_e\epsilon_0$, where n_0 is the electron number density, and s denotes the different ion species in the plasma. Another important effect is the Debye shielding effect, where a bare charge inserted into a plasma instigates charged particle motions that act to attenuate the potential of the charge. This has a characteristic length of $\lambda_D = \left(\omega_{pe}^2/v_{eth}^2 + \sum_s \omega_{pq_s}^2/v_{q_s th}^2\right)^{-1/2}$, known as the "Debye–Hückel screening length" or simply the "Debye length", where $v_{e,q_s th}$ is the thermal velocity of the electrons/ions.

In fully ionized plasma, the only collisions we need to concern ourselves with are Coulomb collisions. Consider a single test particle with charge q_1 traveling with velocity $\mathbf{v}_1$ through a "field" of scattering particles with charge q_2; the Rutherford scattering problem [23]. The frequency of interactions is:

$$\nu_{coll}(1,2) = \frac{n_0}{2\pi}\left(\frac{q_1 q_2}{\epsilon_0 \mu}\right)^2 \ln\left(\frac{\lambda_D}{b_{90}}\right)\frac{1}{|\mathbf{v}_1 - \mathbf{V}_{CM}|^3}, \tag{1}$$

where $\mathbf{V}_{CM}$ is the center-of-mass velocity, $\mu = (m_1 + m_2)/m_1 m_2$ is the reduced mass, n_0 is the number density of scatterers and b_{90} is the 90° scattering impact parameter, with the scattering angle of a single Coulomb collision between particles 1 and 2 with impact parameter b, given by: $\tan(\theta/2) = q_1 q_2/4\pi\epsilon_0 \mu b|\mathbf{v}_1 - \mathbf{V}_{CM}|^2$. For electrons scattering from ions, setting $\theta = 90°$ we obtain $\langle b_{90}\rangle = q_e q_i/4\pi\epsilon_0\mu_{ei}\langle|\mathbf{v}_e - \mathbf{V}_i|^2\rangle$, with the velocity average being $\langle|\mathbf{v}_e - \mathbf{V}_i|^2\rangle = 3k_B T_e/m \equiv 3v_{eth}^2$ [24], yielding $\langle b_{90}\rangle \simeq Ze^2/12\pi\epsilon_0 m_e v_{eth}^2$. Here, a cumulative number of small angle scattering events equivalent to a 90° deflection is considered to be the characteristic "collision". The collision frequency is therefore not the inverse of the time between particle interactions, but more the time for a typical 90° deflection to occur through multiple scattering events.

In an *ideal* plasma, small angle deflections due to numerous simultaneous interactions are by definition [8] the most important. The Debye screening length, λ_D, is intrinsically linked to the collisional behavior of the plasma, as it turns out that the ratio of the cross sections for cumulative small angle scattering (equivalent to a single 90° scatter) to large angle scattering (greater than 90° in a single deflection) is proportional to $\ln(\lambda_D/\langle b_{90}\rangle) = \ln[(9/Z)(4\pi/3)n_e\lambda_D^3] = \ln(9N_D/Z) \equiv \ln\Lambda_{ei}$. Moreover, the average electron–ion collision frequency, $\langle\nu_{ei}\rangle$ (an important reference collision timescale) can be shown to be related to ω_p and $\ln\Lambda_{ei}$, the Coulomb logarithm for electron–ion interactions, by [24]:

$$\frac{\langle\nu_{ei}\rangle}{\omega_p} = \sqrt{\frac{2}{\pi}}\frac{\ln\Lambda_{ei}}{\Lambda_{ei}}, \tag{2}$$

which is valid provided there are numerous ions in a sphere of radius λ_D; the Debye sphere ($N_i \simeq N_D/Z = \Lambda_{ei}/9 > 1$). Fig. 1 shows collisionality for various plasma conditions. We may assume that for sufficient numbers of ions in a Debye sphere the collision frequency will become negligibly small compared with the plasma frequency, which implies we may consider it to exhibit collisionless behavior. The plasma in this limit obeys the Vlasov equation for each species s:

[5] lle.rochester.edu.
[6] hiper-laser.org.

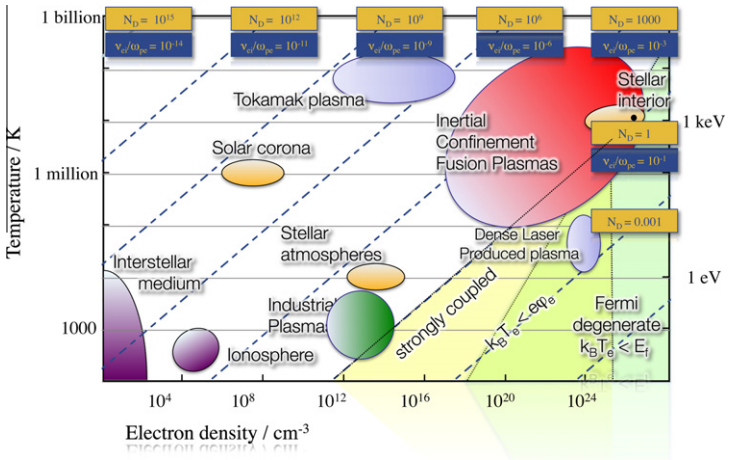

Fig. 1. The relationship between relative collisionality ν_{ei}/ω_p and number of particles in a Debye sphere on a density–temperature phase-space for plasmas.

$$\left[\frac{\partial}{\partial t}+\mathbf{v}\cdot\nabla+q_s(\mathbf{E}+\mathbf{v}\times\mathbf{B})\cdot\frac{\partial}{\partial\mathbf{p}}\right]f_s(\mathbf{p},\mathbf{r},t)=0, \tag{3}$$

where $\mathbf{v}=\mathbf{p}/\sqrt{m_s^2+|\mathbf{p}|^2/c^2}$ and $\mathbf{E}$ and $\mathbf{B}$ are 'macroscopic' electromagnetic fields, either arising external to the plasma or due to the smooth distribution function. For hot plasma ($T_e > 36Z^2$ eV [24]), the uncertainty regarding the path of the particle $\Delta x \gtrsim \hbar/p$ can be larger than the 90° impact parameter. Taking this into consideration results in a quantum correction to the Coulomb logarithm:

$$\Lambda_{ei}^{QM}=\left(\frac{36Z^2e}{k_BT_e}\right)^{1/2}\Lambda_{ei}. \tag{4}$$

2.2. Hot dense plasma

As Λ_{ei} gets smaller, collisions become increasingly important, or alternatively, perhaps we are considering timescales which are large compared with the inverse collision frequency. In this case, we need to consider the effect of interactions within the Debye sphere, and for this the Fokker–Planck equation [25,26] for small angular deflection $1/r^2$ interactions is appropriate to describe the plasma [27,28], under the assumptions that the plasma is not far from equilibrium, that perturbations are slow compared with the plasma frequency, and that there are many particles in a Debye sphere (the latter of which is also of course necessary for the validity of the Vlasov equation) and is accurate to order $\mathcal{O}(1/\ln\Lambda_{ei})$ [24] (inclusion of higher order terms of the Taylor expansion that extend the validity of the Fokker–Planck equation to smaller values of $\ln\Lambda_{ei}$ were considered by Li and Petrasso [29]). The Fokker–Planck equation describes a combination of advection and diffusion in velocity space, and is basically a truncated Taylor expansion of the statistically averaged effect of small angle deflections in velocity space:

$$\frac{\delta f_s}{\delta t}=-\frac{\partial}{\partial\mathbf{p}}\cdot\left\{f_s(\mathbf{p},\mathbf{r},t)\left\langle\frac{\Delta\mathbf{p}}{\Delta t}\right\rangle\right\}+\frac{1}{2}\frac{\partial}{\partial\mathbf{p}}\frac{\partial}{\partial\mathbf{p}}:\left\{f_s(\mathbf{p},\mathbf{r},t)\left\langle\frac{\Delta\mathbf{p}\Delta\mathbf{p}}{\Delta t}\right\rangle\right\}. \tag{5}$$

The coefficient of dynamical friction $\langle\Delta\mathbf{p}/\Delta t\rangle$ represents the slowing down of fast particles and the acceleration of slow particles towards the mean momentum with an average momentum deflection $\Delta\mathbf{p}$ due to multiple, simultaneous, small angle Coulomb collisions for an ensemble of particles moving with momentum $\mathbf{p}$. Similarly, the coefficient of dynamical diffusion, $\langle\Delta\mathbf{p}\Delta\mathbf{p}/\Delta t\rangle$, describes how collisions tend to diffuse the range of momenta of the particle ensemble.

For laser interactions with solid density materials, the plasma is not everywhere well described either by the Vlasov or Fokker–Planck equations, as in regions of cooler, high density material N-body short-range Coulomb interactions become significant, $\omega_p/\langle\nu_{ei}\rangle \ll 1$, but in the lower density, hotter, ablated plasma the plasma will be more Vlasov-like $\omega_p/\langle\nu_{ei}\rangle \gg 1$, Fig. 2. There will also be some region where both 2-body collisions and collective effects are both important in the timescale of interest $\omega_p/\langle\nu_{ei}\rangle \gtrsim 1$. In general, neither the Vlasov equation nor the Fokker–Planck equation is an accurate representation of the particle kinetics.

However, the Debye–Huckël screening effect gives us a way of melding the two equations; for interactions much further than a Debye length, screening implies that a particle does not experience bare charge Coulomb fields and so the ensemble behaves in a Vlasov-like manner. Within a Debye sphere, we may assume that the particles experience individual collisions described by the Fokker–Planck equation [24]. The overall change in the distribution function can be described by the linear combination of the two equations — *the Vlasov–Fokker–Planck equation*:

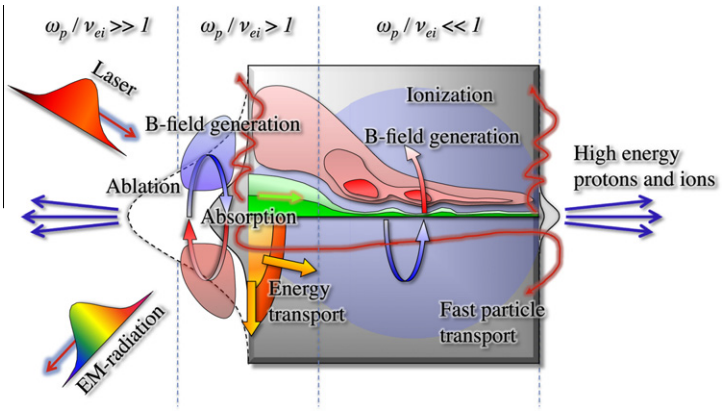

Fig. 2. The physics of high power laser interactions with solid targets.

$$\frac{\partial f_s}{\partial t} + \mathbf{v}\cdot\nabla f_s + \frac{q_s}{m_s}(\mathbf{E}+\mathbf{p}\times\mathbf{B})\cdot\frac{\partial f_s}{\partial \mathbf{p}} = -\frac{\partial}{\partial \mathbf{p}}\cdot\left\{f_s\left\langle\frac{\Delta\mathbf{p}}{\Delta t}\right\rangle\right\} + \frac{1}{2}\frac{\partial}{\partial\mathbf{p}}\frac{\partial}{\partial\mathbf{p}}:\left\{f_s\left\langle\frac{\Delta\mathbf{p}\Delta\mathbf{p}}{\Delta t}\right\rangle\right\}. \tag{6}$$

When combined with Ampère–Maxwell's and Faraday's laws,

$$\nabla\times\mathbf{B} = \mu_0\mathbf{j} + \frac{1}{c^2}\frac{\partial\mathbf{E}}{\partial t}, \tag{7}$$

$$\nabla\times\mathbf{E} = -\frac{\partial\mathbf{B}}{\partial t}, \tag{8}$$

where the current density $\mathbf{j} = \sum_s q_s \int f_s \mathbf{v} d^3\mathbf{p}$ is found from the velocity averages of the distribution functions, this system provides one of the most accurate representation of an *ideal classical plasma* conceivable without explicitly calculating the full N-body interactions for the constituents. In the highest density, coolest regions of the solid, where $\omega_p/\langle\nu_{ei}\rangle \ll 1$, the Debye sphere is smaller than the inter-particle spacing and collective behavior effects are negligible; this is known as a non-ideal, or "strongly coupled" plasma. In solid density material, "warm dense matter", the plasma will generally also no longer be a classical plasma either, as quantum mechanical effects may become important.

In an inertial confinement fusion plasma, although sufficiently hot to neglect quantum effects over the majority of the interaction, the compressed fuel in particular is a quantum mechanical system. This is because the isentrope parameter, $\alpha_F = p_e/p_F$, the ratio of thermal pressure to Fermi degeneracy pressure, is by design as small as possible — the National Ignition Facility design aims for $\alpha_F = 1$ — since the goal is compression [30]. In this case, significant effort must be expended calculating the equation of state.

2.3. Scales in inertial confinement fusion plasma and numerical modeling

The various time and space scales in inertial confinement fusion plasma are of interest when formulating analytic models to describe the dynamics, but are also particularly important for numerical models involving finite time-step integrators. The most important timescales in plasma are the inverse of the electron and ion plasma (angular) frequencies, ω_{pe} and ω_{pi}, the gyro-frequencies $\omega_{ce} = e|B|/m_e$ and $\omega_{ci} = q_s|B|/m_s$ (for magnetized plasma) and various collision timescales, the most important of which is the velocity dependent electron–ion collision frequency, ν_{ei}. When considering the laser–plasma interaction specifically, additional timescales are the inverse of the laser frequency, ω_0 and the pulse duration τ_L.

One significant hurdle to numerically modeling laser–solid interaction plasmas is the multiple time and space scales involved. The National Ignition Facility has long-pulse lasers with duration of the order 10^{-8} s, which is representative of the full interaction timescale we could consider, but the shortest timescales of interest include the laser period, of the order 10^{-15} s, the inverse electron plasma frequency in the compressed core, of the order 10^{-18} s, or the velocity-averaged electron–ion collision timescale [24], of the order 10^{-16} s for a $\sim$10 keV electron temperature in the compressed core [7]. The ratio between the largest and smallest timescales is therefore $\sim 10^{10}$. There is a similar span in spatial scales; the largest spatial scale of interest is the hohlraum or capsule size, of the order 10^{-2} m, whereas microinstabilities may have a scale length of the order c/ω_{pe}, which in the solid density region may be $\sim 10^{-9}$ m, or, alternatively, resolving the electron Debye length v_{th}/ω_{pe} will require even finer resolution.

Generally, studies using Vlasov–Fokker–Planck models have, due to the high computational demands, focused on a smaller region in configuration space rather than a full scale numerical simulation. In a typical hohlraum implosion, there are broadly speaking three regions of interest where kinetic effects are important: (a) the laser entrance hole, where the lasers enter the hohlraum, (b) the hohlraum wall, where laser heating occurs and (c–d) the fuel capsule itself; (c) at the ablation

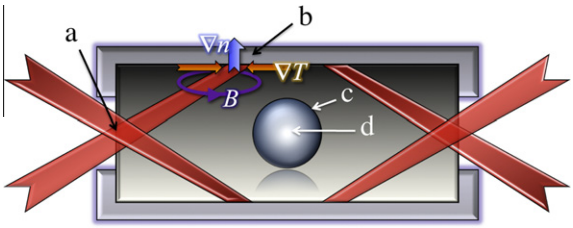

Fig. 3. Kinetic considerations in an implosion in a hohlraum, as for example used on the National Ignition Facility. (a) Instabilities at the laser entrance hole. (b) Nonlocal laser heating and magnetic field dynamics at the hohlraum walls. (c) Plasma ablation from fuel capsule walls. (d) Preheat, shock propagation in the fuel capsule.

Table 1
Reference parameters in different regions of a hohlraum driven implosion with 300 eV radiation temperature. *Source:* Adapted from [6,30,7].

Region	n_e (cm^{-3})	T_e	$\overline{Z}$	λ_D (nm)	Λ_{ei}[a]
(a)	10^{20}	20 keV	5	100	2×10^5
(b)	10^{21}	5 keV[b]	79	20	2000
(c)	10^{23}	300 eV	5	0.4	50
(d) Preheat	10^{20}	300 eV	1	10	3000
(d) Comp.	10^{26}	10 keV	1	0.07	90
	v_{eth} (ms^{-1})	ω_{pe} (s^{-1})	ν_{ei} (s^{-1})	λ_{mfp}	L_{n_e}
(a)	6×10^7	6×10^{14}	7×10^9	8 mm	10 mm
(b)	3×10^7	2×10^{15}	5×10^{12}	6 μm	100 μm
(c)	7×10^6	2×10^{16}	1×10^{15}	7 nm	100 μm
(d) Preheat	7×10^6	6×10^{14}	5×10^{11}	10 μm	100 μm
(d) Comp.	4×10^7	6×10^{17}	2×10^{15}	20 nm	10 μm

[a] Includes quantum correction calculated according to Eq. (4).
[b] Approximate electron temperature at quarter-critical surface [6]. Only one significant figure is given except for $\overline{Z}$. The regions are depicted in Fig. 3.

front and (d) within the capsule where preheat and shock propagation may be considerations (see Fig. 3). In Table 1, some characteristic reference time and space scales and macroscopic parameters are listed for these regions.

For region (d), the table has two entries labelled "preheat" and "comp." (compressed). These are representative values in (preheat) the initial stages of the heating of the capsule, with the density being that of the deuterium–tritium fuel vapor and the temperature that of the X-ray drive for reference and (comp.) being the conditions at the final stages of compression. Here, $v_{eth} = \sqrt{k_B T_e / m_e}$ is the electron thermal velocity, and $\lambda_{mfp} = v_{eth}/\nu_{ei}$ is the mean free path of a thermal electron. L_{n_e} is a qualitative estimate of the scale-length of typical density variations in this region.

As can be seen from the table, the Vlasov–Fokker–Planck equation is expected to be a *valid* description in all areas of interest as $\Lambda_{ei} \gg 1$. However, for regions (c) and (d) when compressed in particular, the value of $\ln\Lambda_{ei}$ is not significantly larger than 1. Since the accuracy of the Fokker–Planck operator is to order $\mathcal{O}(1/\ln\Lambda_{ei})$ the validity of numerical results in these regions will be questionable and an alternative approach, for example using a fluid model, may be more appropriate. Conversely, we can observe that a kinetic description is likely to be necessary for electrons at the walls of the hohlraum — at least near to the critical surface where the laser deposits its energy — and in the fuel capsule in the early stages of heating, since the mean-free-path of electrons is long relative to the gradient scale lengths, which means transport will be delocalized. At the laser entrance hole, the collision time is very long and we may consider a collisionless description to be adequate.

There are two predominant approaches to numerically modeling plasma described by the Vlasov–Fokker–Planck equation; finite difference methods and finite particle methods. To finite difference the full six dimensional phase space of the Vlasov distribution including the Fokker–Planck operator can be computationally difficult due to the rapid increase in calculations required with the number of grid-points used, which means for any realistic problem a direct approach is restrictive. However, fine-scale angular information in the momentum distribution function is generally smoothed away by collisions. Hence, one early approach to numerical methods was to expand the distribution function in terms of a series of spherical basis functions. However, whether finite-difference or finite-particle, one of the problems with kinetic methods is the increased amount of calculations that need to be performed to model the momentum space behavior compared with hydrodynamic models. The Fokker–Planck part of the equation is also integro-differential, in principle further increasing the number of numerical calculations. These together are restrictive in terms of computing power, and it was not until the 1980s when serious attempts to perform Vlasov–Fokker–Planck numerical calculations were attempted.

2.4. Notation

The notation used throughout is that we use bold fonts to represent vector quantities, e.g. **B**, and a double underscore to represent rank 2 tensor quantities, e.g. $\underline{\underline{P}}$. Contractions obey the rule that for a tensor with components i and j, e.g. P_{ij}, a

centered dot contracts nearest indices, e.g. the dyadic tensor $\nabla\mathbf{A}$ contracted with $\mathbf{B}$ in the form $(\nabla\mathbf{A})\cdot\mathbf{B}$ is equivalent to $\sum_j(\nabla_i A_j)B_j$. Dots arranged vertically, e.g. :, represent the tensor contraction, so for two dots, $\underline{\underline{A}}:\underline{\underline{B}}$ is equivalent to $\sum_{i,j}A_{ij}B_{ij}$. We also identify the ith component of a vector $\mathbf{A}$ as A_i, and for a tensor of n dimensions, $\mathbf{A}$, the $a_1, a_2, \ldots, a_n$th component is given by $A_{a_1,a_2,\ldots,a_n}$. Also used is the Einstein sum convention $A_iA_i = \sum_i A_iA_i$, $A_{ij}A_{ik} = \sum_i A_{ij}A_{ik}$, etc.

For finite differenced equations, superscript indices, e.g. x^n, indicate finite differenced time steps, $x^{n+1} = x(t_n + \Delta t)$, where $t_n = t_{n-1} + \Delta t_{n-1/2}$ and $\Delta t_{n-1/2}$ is the spacing between the t_{n-1} and t_n times. Likewise, subscript indices, e.g. $x_{i,j}$, indicate finite differenced spatial variables, in both position and momentum spaces, $f_{i,j,k} = f(x_i, y_j, p_k)$, with x_i, y_j and p_k defined in a similar way to the time grid points. The use of i and j for spatial coordinates, and k for the momentum (magnitude) coordinate will be used throughout.

3. The Fokker–Planck operator

The quantities in the Fokker–Planck equation: $\langle\Delta\mathbf{p}\rangle$ and $\langle\Delta\mathbf{p}\Delta\mathbf{p}\rangle$ are defined by:

$$\langle\Delta\mathbf{p}\rangle = \int \psi(\mathbf{p},\Delta\mathbf{p})\Delta\mathbf{p}d(\Delta\mathbf{p}), \tag{9}$$

$$\langle\Delta\mathbf{p}\Delta\mathbf{p}\rangle = \int \psi(\mathbf{p},\Delta\mathbf{p})\Delta\mathbf{p}\Delta\mathbf{p}d(\Delta\mathbf{p}), \tag{10}$$

where $\psi(\mathbf{p}, \Delta\mathbf{p})$ is the probability that in a time Δt an electron will be deflected by an amount $\Delta\mathbf{p}$ to a new momentum $\mathbf{p}$ from $\mathbf{p} - \Delta\mathbf{p}$. The quantities in the angled brackets give the averages of the deflection $\Delta\mathbf{p}$ and the dyadic product $\Delta\mathbf{p}\Delta\mathbf{p}$. To evaluate these for a plasma, we can consider the interaction, between a particle of mass m_s with initial momentum $\mathbf{p}_s$ and a second particle with mass m_t and initial momentum $\mathbf{p}_t$ for the particular case of a Coulomb interaction.

Following Chandrasekhar's influential review paper [27], Rosenbluth, MacDonald and Judd studied the Fokker–Planck equation for an inverse square law in particular to make it amenable to numerical calculation [28]. They cast the Fokker–Planck operator (in its non-relativistic form — for a relativistic formulation see e.g. [31]) for collisions of species s on species t in terms of potentials h_s and g, in the form:

$$\frac{1}{\Gamma_{st}}\left.\frac{\delta f_s}{\delta t}\right|_t = -\frac{\partial}{\partial\mathbf{p}}\cdot\left(f_s\frac{\partial h_s}{\partial\mathbf{p}}\right) + \frac{1}{2}\frac{\partial^2}{\partial\mathbf{p}\partial\mathbf{p}}:\left(f_s\frac{\partial^2 g}{\partial\mathbf{p}\partial\mathbf{p}}\right), \tag{11}$$

where the potentials are defined through the relations:

$$\frac{\partial}{\partial\mathbf{p}}\cdot\frac{\partial}{\partial\mathbf{p}}h_s = -4\pi\sum_t\frac{m_s + m_t}{m_t}f_t(p), \tag{12}$$

and

$$\left(\frac{\partial}{\partial\mathbf{p}}\cdot\frac{\partial}{\partial\mathbf{p}}\right)\left(\frac{\partial}{\partial\mathbf{p}}\cdot\frac{\partial}{\partial\mathbf{p}}\right)g = -8\pi\sum_t f_t(p), \tag{13}$$

and $\Gamma_{st} = 4\pi q_s^2 q_t^2 \ln\Lambda_{st}/m_s$, where the Coulomb logarithm, $\ln\Lambda_{st}$, is the logarithm of the ratio of the Debye length to the small impact parameter discussed above, representing the limits of the integration over b for species s colliding with species t. These 'potentials' in momentum space are somewhat analogous to potentials in position space in electromagnetism.

Another formulation of the Fokker–Planck equation for plasma evolved from Landau's proposed description of plasma based on the Boltzmann equation assuming small angle scattering [32,33]. This alternative form of the equation is:

$$\frac{2}{\Gamma_{st}}\left.\frac{\delta f_s}{\delta t}\right|_t = \frac{\partial}{\partial\mathbf{p}}\cdot\left[\int\frac{d^3\mathbf{p}'}{|\mathbf{p}'-\mathbf{p}|}\left(\underline{\underline{\mathbb{I}}} - \hat{\mathbf{u}}\hat{\mathbf{u}}\right)\left\{\frac{f_s(\mathbf{p})}{m_t}\frac{\partial f_t(\mathbf{p}')}{\partial\mathbf{p}'} - \frac{f_t(\mathbf{p}')}{m_s}\frac{\partial f_s(\mathbf{p})}{\partial\mathbf{p}}\right\}\right], \tag{14}$$

where $\hat{\mathbf{u}}$ is a unit vector in the direction $\mathbf{p}' - \mathbf{p}$. This formulation is known as the *Fokker–Planck–Landau* collision operator.

3.1. Key algorithm development: Numerical methods for the Fokker–Planck equation

Numerical solutions of the Fokker–Planck equation using straightforward non-conserving finite difference schemes were initially attempted for studying a number of plasma systems. One of the earliest works was MacDonald, Rosenbluth and Chuck's numerical study of the relaxation of a beam-like plasma distribution to a Maxwellian [34]. Other studies include hydrogen plasma heated by neutral beam injection [35], end losses from a mirror machine [36], partial ionized plasma [37] and other phenomena [38,39]. These required fine gridding to gain accurate solutions, and the operator can be numerically difficult to handle in many dimensions for a Cartesian system, because it is not a natural coordinate system for the collision operator.

One of the difficulties with forming a conservative finite-difference scheme for the Fokker–Planck equation is the intrinsic three dimensional nature of collisional behavior. However, collisions tend to push a distribution function towards isotropy

and so a spherical system or expansion in terms of angular basis functions such as spherical harmonics is convenient. It reduces the momentum space dimensionality to one dimension – albeit with an infinite series of terms resulting from the expansion – which makes the coupled set of integro-differential equations more amenable to numerical solution. For collisional plasma it may be a reasonable approximation to truncate this expansion since collisions tend to smooth momentum space anisotropy.

For an infinite, fully ionized plasma close to isotropy, if we merely consider energy relaxation between electrons and ignore momentum isotropization — caused by electron–electron and electron–ion collisions — we end up with the zero order term of an expansion in momentum space of Rosenbluth's Fokker–Planck operator [40] in spherical harmonics [41,37] or Cartesian tensors [42]. This can then cast in a much simpler form (we use a nonrelativistic formulation in terms of velocity here):

$$\frac{1}{\Gamma_s}\frac{\delta f_{s0}}{\delta t} = \frac{1}{v^2}\frac{\partial}{\partial v}\left[C(f_{s0})f_{s0} + D(f_{s0})\frac{\partial f_{s0}}{\partial v}\right], \tag{15}$$

where f_{s0} is the isotropic part of the distribution function f_s — and the lowest order term in the spherical harmonic expansion — and v is the magnitude of velocity $\mathbf{v} = \mathbf{p}/m$,

$$C(v,\mathbf{r},t) = 4\pi\int_0^v f_0(u,\mathbf{r},t)u^2 du \tag{16}$$

and

$$D(v,\mathbf{r},t) = \frac{4\pi}{v}\int_0^v u^2\left[\int_u^\infty f_0(w,\mathbf{r},t)w dw\right]du. \tag{17}$$

This set of equations — but applying finite differencing to an expanded form of the integral, $D(v,\mathbf{r},t) = \frac{4\pi}{3}\left[\frac{1}{v}\int_0^v f_0(u)u^4 du + v^2\int_v^\infty f_0(u)u du\right]$ — was considered numerically by Chang and Cooper in a way that conserves the number of particles in their influential paper [43]. Their algorithm starts with a linearized implicit differenced scheme with center differenced velocity derivatives, which are then shifted towards forward differencing through an equilibrium seeking algorithm which ensures positivity and conservation of particle number along with accuracy of the equilibrium solution. The finite difference form of the equation is given in terms of "generalized currents" $F = Cf + D\partial f/\partial v$ in the conservative finite difference form (dropping the species index):

$$\frac{1}{\Gamma\Delta t}\left(f_k^{n+1} - f_k^n\right) = \frac{1}{v_k^2\Delta v}\left(F_{k+1/2}^{n+1/2} - F_{k-1/2}^{n+1/2}\right), \tag{18}$$

where the $n + 1/2$ superscript indicates that $F^{n+1/2}$ is some combination of terms at n and $n + 1$ (C and D are taken at n to linearize the equation). It is clear from the finite difference form of Eq. (18) that the v^2 moment (i.e. particle density — see subSection 4.1) will be conservative for appropriate boundary conditions. The numerical velocity derivative in the second term of $F_{k+1/2}^{n+1/2}$ can easily be center differenced using combinations of f_{k+1}^{n+1} and f_k^{n+1}, but the first term, $C_{k+1/2}^n f_{k+1/2}^{n+1}$ requires some interpolation between f_{k+1}^{n+1} and f_k^{n+1}. Clearly, the most obvious choice is $f_{k+1/2} = \left(f_{k+1}^{n+1} + f_k^{n+1}\right)/2$, but Chang and Cooper show that in general this can result in negative f [43]. The key step to ensuring positivity is to take $f_{k+1/2}^{n+1} = \delta_k f_{k+1}^{n+1} + (1-\delta_k)f_k^{n+1}$, and calculate δ_k from the requirement that the equilibrium solution of the finite differenced flux $F_{k+1/2}^{n+1/2}$ is equivalent to the analytic solution, $f(v) = f(0)\exp(-\int_0^\infty [C(v')/D(v')]dv')$, resulting in:

$$\delta_k = \frac{D_{k+1/2}^n}{C_{k+1/2}^n\Delta v} - \left(\exp\left[\frac{C_{k+1/2}^n\Delta v}{D_{k+1/2}^n}\right] - 1\right)^{-1}. \tag{19}$$

Using such an "equilibrium seeking" weighting was shown to ensure $f_k^{n+1} \geqslant 0$ [43]. Larsen et al. [44] subsequently showed that this scheme can break down for far from equilibrium problems, and generalized the scheme to allow larger time steps and the ability to solve strongly nonlinear problems. Much later, Buet and Dellacherie [45] showed that an *explicit* version of Chang and Cooper's algorithm [43] is positive and entropy satisfying for a certain Courant–Friedrichs–Lewy condition and will converge towards a discrete equilibrium solution.

Although Chang and Cooper's scheme [43] conserves particle number, it does not conserve energy. Bobylev and Chuyanov initially suggested a method for expressing the equation in completely conservative form [46], and later a modification to the numerical model introduced by Langdon [47], demonstrated by Kho [48] and later improved by Epperlein [49] allowed the algorithm to conserve energy, and Epperlein later developed the algorithm in one dimension (i.e. velocity magnitude v) to be both implicit and energy conserving [50]. The important step that allowed energy conservation was expressing the integral D in the form given in Eq. (17), where D is calculated from $\partial(vD)/\partial v$, instead of the analytically equivalent form used by Chang and Cooper [43]. Degond Lucquin–Desreux [51] and Buet et al. [52] also developed a number of fast algorithms for solving the Fokker–Planck–Landau equation that conserve mass, energy and decrease entropy. Lemou and Mieussens [53] later developed a similar but implicit scheme.

These schemes are reasonable for plasma close to isotropy, but for strongly anisotropic distribution functions, higher order expansion of the Fokker–Planck operator is required. Alouani-Bibi et al. [54] studied the isotropic Fokker–Planck collision

operator alone in comparison to the inclusion of the anisotropic parts of the expansion. A full 3D phase space finite difference collision operator was also compared, and demonstrated that the "semi-anisotropic" operator gave good agreement with the full 3D finite difference operator, but the isotropic operator was in error. An analogous anisotropic expansion of the Fokker–Planck operator was also recently included by Tzoufras and Bell in the Oshun code [55]. Chacón et al. studied the Fokker–Planck operator in two dimensions [56,57] and developed an implicit and energy conserving algorithm by reformulating the friction term in the Fokker–Planck collision operator by considering the analogue of the h_s potential with the Maxwell stress tensor. Spectral methods for solving the Fokker–Planck equation were also introduced by Pareshchi et al. [58]. More recently, methods for solving the Fokker–Planck equation for inhomogeneous plasmas [59], and magnetized plasma [60] have been developed.

3.2. Implicit and conservative differencing scheme for the Fokker–Planck equation

Epperlein introduced an implicit and conservative differencing scheme for the Fokker–Planck equation [50] using modifications due to Langdon [47], demonstrated by Kho [48], which improved on Chang and Cooper's scheme [43] by conserving energy as well as particle number, in addition to being implicit.

Implicit finite time differencing of Eq. (15) (dropping the subscripts indicating species for clarity) results in:

$$\frac{f^{n+1}-f^n}{\Delta t} = F^{n+1} \equiv \frac{\Gamma}{v^2}\frac{\partial}{\partial v}\left[C^{n+1}f^{n+1} + D^{n+1}\frac{\partial f}{\partial v}^{n+1}\right]. \tag{20}$$

The nonlinear terms must be dealt with in some way, with the standard approach, as in for example Ref. [43], being to perform nonlinear iterations of f_{s0}, C and D. The problem is that while analytically the energy moment of the two terms on the right hand side of Eq. (15) cancel, the numerically calculated terms at different iterations do not and can result in large errors [50]. An approach to obtain precise energy conservation [47,48] is to eliminate the nonlinear terms by considering a truncated Taylor expansion of the collision operator F^{n+1} in time $F^{n+1} = F^n + \partial F/\partial t|^n \Delta t + \mathcal{O}(\Delta t^2)$. Epperlein here then expresses $\partial F/\partial t|^n \Delta t \equiv (\partial F/\partial f)^n (f^{n+1} - f^n)$, with $F = F(f)$, which renders the expression equivalent to that in Briley and McDonald [61] for an equation of the form $\partial\phi/\partial t = F(\phi)$, where terms of order Δt^2 and higher are neglected in order to linearize the equation in time. This does not appear to be analytically rigorous, as in the case considered here F is also a function of $\partial f/\partial v$ and $\partial^2 f/\partial v^2$. However, although it is not explicitly stated, if the integral and differential v operators are expressed as linear algebraic operators arising from as yet undetermined finite difference approximations of the differential operators, then Eq. (20) can be written in the finite difference form:

$$\left[\frac{1}{\Delta t} - \left(\frac{\partial F}{\partial f}\right)^n\right](f^{n+1} - f^n) = F^n, \tag{21}$$

where $(\partial F/\partial f)^n f^{n+m}$ is:

$$\left(\frac{\partial F}{\partial f}\right)^n f^{n+m} = \frac{\Gamma}{v^2}\frac{\partial}{\partial v}\left[C^{n+m}f^n + C^n f^{n+m} + D^{n+m}\frac{\partial f}{\partial v}^n + D^n\frac{\partial f}{\partial v}^{n+m}\right], \tag{22}$$

with m being either 1 or 0. The same result can be obtained directly using the partial time derivative. The equation has now been linearized and can be solved implicitly. The velocity derivatives are taken as cell centered initially, as in the Chang–Cooper scheme [43], with the same iterated δ coefficient but with C and D calculated numerically from:

$$C_{k+1/2} = \sum_{l=1}^{k} \Delta v_l v_l^2 f_l, \tag{23}$$

$$(vD)_{k+1/2} = (vD)_{k-1/2} + \Delta v_k v_k^2 \sum_{l=k}^{K-1} \Delta v_{l+1/2}\, v_{l+1/2} f_{l+1/2}. \tag{24}$$

This scheme exactly conserves energy as well as charge density, and ensures positivity.

4. Origins in ablative drive

Some of the first calculations using a full Vlasov–Fokker–Planck code were to look at the problem of heat fluxes in the presence of steep temperature gradients in plasma, relevant to the ablating plasma in inertial confinement fusion. It was known for a long time that in steep gradients the mean-free-path of a thermal electron becomes relatively large, and therefore downstream of the high temperature the distribution function gains a hot 'tail' from the less collisional electrons, leading to non-Maxwellian distributions [62]. This effect is known as 'nonlocal transport' [63,14,64–69], as the electrons are delocalized so that the bulk properties of the plasma at a point in space are significantly affected by the properties of the plasma some distance away.

Another way of looking at this is that the plasma version of Fick's diffusion law [70] due to Spitzer and Härm [71], $\mathbf{q}_{SH} = -\kappa\nabla T_e$ may lead to a heat-flux that is greater than the free streaming limit — equivalent to all electrons traveling down

the temperature gradient with the thermal velocity — which is clearly unphysical as this would lead to gross departures from quasineutrality over regions much greater than the Debye length. In hydrodynamic codes, flux-limiters were initially introduced to prevent the heat flux exceeding this limit [62,72]. The flux-limiter is not calculated a priori, and a variety of values have been advocated to obtain agreement between fluid modelling and experimental results.

Methods to introduce nonlocal effects to a fluid code through a convolution of a kernel representing the hot electron population [73–76] — more recently formulated in conjunction with magnetic field effects [77–79] — or using a Bhatnagar–Gross–Krook [80] type collision operator [81–84] were also introduced later. The latter method was recently used to demonstrate inhibited transport in the heat pulse and preheat ahead of it [85], similar to the results of Bell et al. [14]. Mason [65] also studied the electron heat transport problem using a Monte-Carlo calculation.

Bell et al. [14] were the first to numerically calculate the full Vlasov–Fokker–Planck equation, studying the problem of nonlocal heat transport using a code in one spatial and one velocity dimension using the f_0 and f_1 terms of the expanded equation (the expansion is described as being in terms of Legendre polynomials in the paper, but this is basically equivalent to an azimuthally symmetric version of either a spherical harmonic or Cartesian tensor expansion [86]). They found that indeed the kinetic calculations indicated strong heat flow inhibition and the breakdown of the Spitzer–Härm heat transport theory [71]. Bell et al. used the Chang and Cooper scheme for the Fokker–Planck part of the equation [43], and an advection scheme due to Cheng and Knorr [87], which also involved a time-splitting algorithm between the advection in position and momentum configuration spaces. Their method shifts the distribution function in three steps; a shift along the x-axis for half a time step, followed by a shift along the v-axis for a whole time step, and finally another half-step shift along the x-axis. The shifted distribution function was then interpolated onto the grid using, in the case of Bell et al., a cubic interpolation.

In their simulation, the left-hand boundary of a uniform plasma was heated rapidly and maintained at a temperature of four times the ambient temperature. The heat from this region was then allowed to flow into the colder background. Fig. 4 shows the heat flow from Bell et al.'s Vlasov–Fokker–Planck calculation at two points in time compared with the equivalent Spitzer–Härm heat flow, both normalized to the free streaming limit $Q_f = nk_BT_e(k_BT_e/m_e)^{1/2}$, as a function of the temperature scale length, $L = T_e(dT_e/dx)^{-1}$ normalized to the electron thermal mean-free-path. The points read from the lower right, up and left then turn back right. Read in this order, they correspond to points along the grid from the start of heated region (lower right) to the edge of the heated region (leftmost point) and then far out to the cooler background plasma (upper right). This figure clearly indicates both strong inhibition of heat flux at the steepest part of the temperature gradient, which determines the overall evolution of the system, to more than an order of magnitude less than the Spitzer–Härm heat flow. Conversely, ahead of the heat front preheating is evidenced in the significantly higher than Spitzer–Härm heat flow far from the heated region.

This study was followed by a number of later investigations using the same basic $f_0, f_1, f_2, \ldots$ expansion Vlasov–Fokker–Planck model [88,89,74]. Epperlein and Haines [90] also discovered errors in Braginskii's transport coefficients [91] using direct Vlasov–Fokker–Planck numerical calculation, and then formulated new analytic transport coefficients as a consequence. Matte et al. also coupled an electron Vlasov–Fokker–Planck code to an ion hydrodynamic code to study further the heat transport problem with comparison to a hydro-code with a flux limiter [92]. This also included laser heating via the inverse bremsstrahlung operator of Langdon [93], which is now a staple of long-pulse laser–plasma simulation. The code, FPI, was later extended to include anisotropic collision operators (a code named FPI+) [54].

In Fig. 5, the density profiles at $t = 0$ and $t = 600$ ps are shown for both the calculation with the Vlasov–Fokker–Planck code and also pure fluid calculations with different flux limiters to match the profile of the kinetic calculation. Matte et al. showed that the usual flux limiter $f = 0.03$ (at that time) was a poor match to the kinetic calculation, and although the profile could be matched in either the corona with $f = 0.15$ or the cooler, dense plasma with $f = 0.08$, a single choice of flux limiter would not

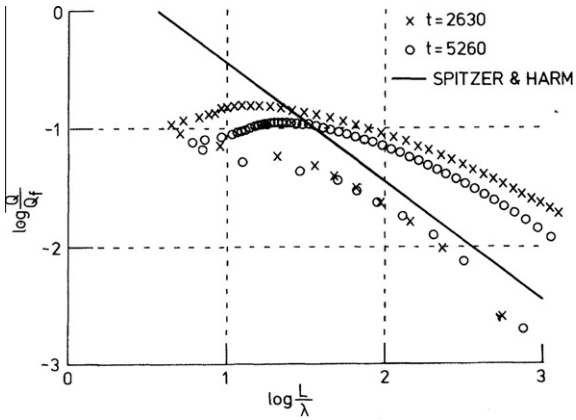

Fig. 4. Bell et al.'s plot of heat flow Q against inverse temperature gradient. $Q_f = nk_BT_e(k_BT_e/m_e)^{1/2}$ is the free streaming limit, λ is the mean free path of an electron with energy $3k_BT_e$, and $L = T_e(dT_e/dx)^{-1}$. All quantities are defined locally. The solid line gives the Spitzer–Härm conductivity for $Z = 4$. *Source:* Reprinted with permission from [14]. Copyright (1981) by the American Physical Society.

agree everywhere. Similar calculations were performed more recently by Li et al. [94], which were extended to higher intensities. They concluded that at higher intensities a time-dependent flux-limiter would be required. Absorption by inverse bremsstrahlung was also studied by Ersfeld and Bell [95] using a Vlasov–Fokker–Planck code to obtain self-consistent electron distributions.

4.1. Key algorithm development: spherical basis function expansions of the distribution function

For problems that are sufficiently collisional, the anisotropic part of the momentum dependence in the distribution be may considered a perturbation to the isotropic component f_0. It is therefore convenient to expand the distribution function in terms of basis functions which contain the angular information, while the momentum magnitude v is retained, hence reducing the dimensionality of the problem. Due to the fact that even for one spatial dimension the momentum space needs to be three dimensional to correctly model collisional effects, this has almost exclusively been the approach for numerical Fokker–Planck modeling. The basis functions are not unique, and different approaches have been used by different authors. Generally, to first order the expansions tend to be the same, but for higher order terms they are different.

Here we will introduce a Cartesian tensor expansion which was first developed when applied to plasma by Johnston and Shkarofsky [86,42,24]. Another valid choice is a spherical harmonic decomposition [96]. However, the Cartesian tensor expansion has an elegant relationship with the physical quantities we encounter such as anisotropic pressure or the heat-flux tensor, which motivates the choice here. In both cases, the expansion basis functions are eigenfunctions of the electron–ion pitch angle scattering collision operator, and are also a natural basis for magnetic rotations.

The general decomposition is of the form:

$$f(\mathbf{p}) = f_0(p) + \mathbf{f}_1(p)\cdot\hat{\mathbf{p}} + \underline{\underline{f}}_2(p) : \hat{\mathbf{p}}\hat{\mathbf{p}} + \cdots, \tag{25}$$

where the momentum unit vectors, $\hat{\mathbf{p}}$, are defined in a spherical polar coordinate system (p, θ, ϕ) in terms of 'direction cosines', which are essentially the cosines of angles measured from each axis of the corresponding Cartesian coordinate system (p_x, p_y, p_z). The relationship between the angles from the axes $(\theta_x, \theta_y, \theta_z)$ and the spherical polar coordinate system is $\cos\theta_x = \sin\theta\cos\phi$, $\cos\theta_y = \sin\theta\sin\phi$, and $\cos\theta_z = \cos\theta$. The unit vector $\hat{\mathbf{p}}$ is defined in terms of these as $\hat{\mathbf{p}} = \cos\theta_x\hat{\mathbf{x}} + \cos\theta_y\hat{\mathbf{y}} + \cos\theta_z\hat{\mathbf{z}}$. The expanded set of equations are shown in the appendix.

This expansion has the same effect of replacing the angular dimensions with the series terms so that the three momentum-space dimensions are reduced to one dimension and an infinite series of terms in the expansion. Since the collisions tend to diffuse fine angular structure, to good approximation most of these terms can then be neglected (although the ordering $f_0 \gg |\mathbf{f}_1| \gg |\underline{\underline{f}}_2| \gg \cdots$ does not necessarily hold for all v). The result is that only a few of the terms are necessary to describe the relevant physics (in a sufficiently collisional plasma) with reasonable accuracy, which drastically reduces the number of computations necessary, but still retains the three dimensional nature of the momentum phase space. If only f_0 and f_1 are retained this is known as the *diffusive approximation*, and is equivalent to the P_1 approximation in neutron kinetics.

The terms in the expanded f can be linked to macroscopic quantities such as density, temperature etc. through momentum moments — weighted integrals over the momentum space of the distribution function. The isotropic term f_0 yields the species number density and internal energy density through the following moments: $n = 4\pi\int_0^\infty f_0 p^2 dp$ and $U = 4\pi\int_0^\infty f_0 p^2(p^2/2m)dp$. Current contributions and (total) heat flow are obtained from moments of the first order anisotropic part f_1 via $\mathbf{j} = (4\pi q/3)\int_0^\infty \mathbf{f}_1 p^2 v dp$ and $\mathbf{q}_T = (4\pi/3)\int_0^\infty \mathbf{f}_1 p^2 v(p^2/2m)dp$. For higher rank tensor quantities, the

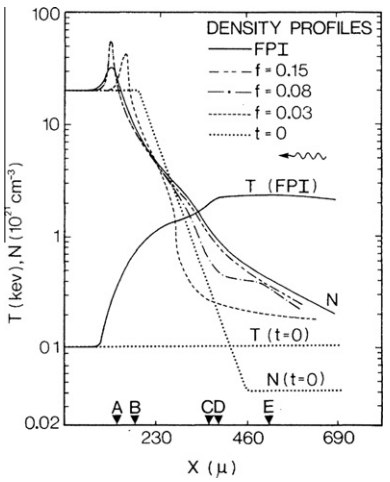

Fig. 5. FPI calculations of heat transport. Density (N) and temperature (T) vs. Eulerian coordinate X. Dotted lines: initial state ($t = 0$). Solid lines: FPI result at 600 ps. Other lines: LILAC density at 600 ps, with three f values. *Source:* Reprinted with permission from [92]. Copyright (1984) by the American Physical Society.

relationship between the Cartesian tensors and these quantities is marginally more direct than when using spherical harmonics. For example, the anisotropic part of the full pressure tensor, $\underline{\underline{P}} = \underline{\underline{\mathcal{I}}}p/3 - \underline{\underline{\Pi}}$ (which includes the scalar pressure $p = 2U/3$) is given by $\underline{\underline{\Pi}} = (4\pi/5)\int_0^\infty \underline{\underline{f}}_2 p^2(p^2/2m)dp$, where $\underline{\underline{\mathcal{I}}}$ is the identity matrix.

4.2. The Courant–Friedrichs–Lewy condition in the Vlasov equation

In their seminal paper, Courant, Friedrichs and Lewy (CFL) [97] demonstrated that for finite difference approximations of hyperbolic partial difference equation, there is a condition on the convergence (and therefore stability) of the solution relating the finite differences, which for an advection equation of the form:

$$\frac{\partial \phi}{\partial t} = C\frac{\partial \phi}{\partial h}, \tag{26}$$

when finite differenced with step sizes Δt and Δh, and with forward differencing in time, the CFL condition is $C\Delta t \leqslant \Delta h$ to ensure convergence of the solution. The Vlasov equation describes advection in position space and momentum space, and therefore in addition to the CFL condition common to spatially dependent problems, $v_{1,2,3}\Delta t \leqslant \Delta r_{1,2,3}$, we also have CFL conditions for advection in momentum space $qE_{1,2,3}\Delta t \leqslant \Delta p_{1,2,3}$ and $q(v_{1,2,3}B_{2,3,1} - v_{2,3,1}B_{1,2,3})\Delta t \leqslant \Delta p_{3,1,2}$, where subscripted numbers indicate orthogonal basis vectors defining the momentum space. Clearly, with the spherical expansion this can become a serious constraint for explicit methods, as the innermost momentum space cells will evidently have a very small spacing in momentum, assuming that the grid is divided up evenly in angle. This limitation was recently overcome within the Kalos framework [96] by using a filtered grid in momentum-space [55].

Solving the advection equations in phase-space and obeying the CFL condition is nontrivial in lieu of a fully implicit scheme. Upwind methods are extremely good ways of solving a constant coefficient advection equation since they preserve particle number, positivity and monotonicity. One method that is used in a number of codes is the Piecewise-Parabolic-Method [98]. A review of these methods in the context of Eulerian Vlasov solvers can be found in [99].

5. Magnetic field generation in inertial confinement fusion

Another problem which has been studied extensively in the context of inertial confinement fusion is spontaneous magnetic field generation and transport by electron fluxes, particularly at the walls of the hohlraum. Magnetic fields are thought to be important in hohlraums as they may result in temperature nonuniformities that increase stimulated Brillouin and Raman scattering of the laser drivers, which can decrease coupling of laser energy to the walls [100]. Magnetic fields also greatly complicate the plasma simulation problem, as they influence in a complex way the electron transport, but are likewise influenced themselves by electron transport.

The electric field that arises to balance pressure gradients in the plasma is rarely curl free (and therefore generates magnetic fields through Faraday's law), and so even in the case of an equilibrated plasma, magnetic fields arise through the $\nabla T_e \times \nabla \ln n_e$ generation mechanism, first proposed in astrophysical scenarios by Biermann [101]. In laser–solid interactions this is naturally significant, as the exponentially decreasing plasma density of the ablation front [102] is perpendicular to the temperature gradients of the circular laser heating region, leading to azimuthal magnetic fields [103,104]. This means they are important in inertial confinement fusion modeling in general. The presence of strong magnetic fields in inertial confinement fusion scenarios has recently been confirmed by measurements in hohlraum and slab target experiments using proton probing [105,106].

When electron kinetic effects are considered, magnetic fields can even be generated in the absence of density gradients by different nonlocal fluxes, as demonstrated by Kingham and Bell [107] using an implicit 2D Vlasov–Fokker–Planck code with magnetic fields, Impact [108] (Fig. 6). In steep gradients, nonlocal transport results in faster electrons and slower electrons diffusing at different rates, leading to different spatial profiles for the different populations, which ultimately leads to an electric field with a nonzero curl. This is in contrast to the local (classical transport) approximation in which, in the absence of currents and density gradients, $\mathbf{E} \propto \nabla T_e$, which always has a zero curl by definition.

Here, we define a magnetized plasma as one where the product of the electron cyclotron frequency, $\omega_{ce} = e|B|/m_e$ and the electron–ion 90° scattering time, τ_{ei}, is larger than unity, $\omega_{ce}\tau_{ei} > 1$. Other constraints could be introduced, such as that the gyro-radius of all particles need to be small compared with typical system scale lengths, but we may be interested in situations where this may not be the case (hence where the transport theory of Braginskii [91] breaks down). The consequence of this condition is that the electron gyroradius, $r_{ce} = |p|/e|B|$ is the dominant scale for electron transport rather than the electron–ion collision mean-free-path $\lambda_{ei} = v_{eth}\tau_{ei}$. In a typical hohlraum, magnetic fields may be expected with magnitudes up to $\sim$100 T [100], or 1 MG, and with electron temperatures ranging up to 5 keV [6] in the gas fill. By this definition, some of the electrons in the hohlraum will be magnetized, $\omega_{ce}\tau_{ei} \sim 4$, for a 100 T field at the quarter critical surface for a 0.35 μm laser of a CH gas fill with $\overline{Z} = 5.3$ and a 5 keV electron temperature. $\overline{Z} = \sum_i n_i Z_i^2/n_e$ is the 'average' atomic number (according to Shkarofsky [24], and is also known as the 'effective' atomic number elsewhere). Conversely, due to the non-uniformity of the magnetic fields there will be regions where the magnetization is $\omega_{ce}\tau_{ei} \ll 1$ but where the collision mean-free-path is

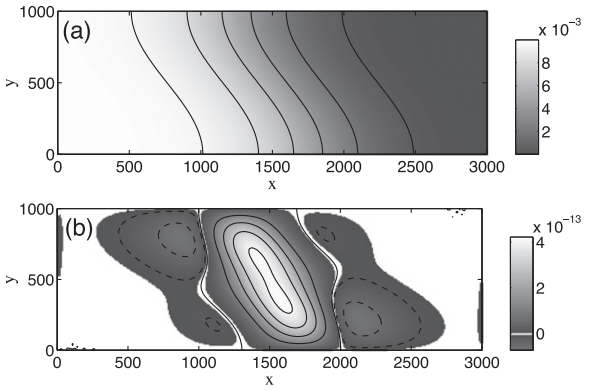

Fig. 6. Kingham and Bell's Vlasov–Fokker–Planck simulation showing magnetic field generation in the absence of density gradients. (a) Initial, non-uniform temperature perturbation causing B-field growth. (b) Nonlocal magnetic field profile at Δt. *Source:* Reproduced from [108].

relatively long. Using the same conditions as above, the mean-free-path is $\lambda_{ei} = 5$ μm. This is non-negligible compared with the typical transport scales in a hohlraum, and means that the assumption of local thermal equilibrium is not valid.

Under these nonlocal transport conditions, there are regions in the plasma where the electron distribution function has a significant nonthermal population of hot electrons. These modify the transport properties and also the generation and advection of magnetic fields in those areas. The interplay between nonlocal transport and magnetic fields is a complex and poorly understood problem [109]. A Vlasov–Fokker–Planck calculation was also used to confirm the transport theory of Ridgers et al. in the presence of both magnetic fields and inverse bremsstrahlung heating [110], similar to those of Braginskii [91] later corrected by Epperlein and Haines [90].

As electrons stream from hotter regions of plasma they also transport the magnetic fields via an effect analogous to the Nernst effect in semiconductors, which arises from the velocity dependence of the collision frequency, which makes it easier for slower electrons to diffuse across magnetic field lines [111–113]. The velocity at which the magnetic fields are advected is related to the electron heat-flux, which is dominated by the faster particles, those with 2–3 times the electron thermal velocity. This was first studied via numerical integration of the Vlasov–Fokker–Planck equation by Kho and Haines [112] and Luciani et al. [113], who both showed that the Nernst effect would advect magnetic fields up the density gradient in a laser–solid interaction with the heat flow, with Kho and Haines concluding that this would drive a convective amplification of the magnetic fields.

Vlasov–Fokker–Planck simulations were later used to explain experimental results using a strong solenoid magnet with laser heated plasma to demonstrate the interplay between nonlocal transport and magnetic fields [115], with the $B = 0$ experimental case calculated using the zero magnetic field Vlasov–Fokker–Planck code Spark [116,117]. Sufficient magnetization of the plasma localizes the plasma electrons in the directions perpendicular to the magnetic field due to the particles being restricted by their gyro-orbits. However, later simulations by Ridgers et al. [114] — using the implicit Vlasov–Fokker–Planck code with self-consistent magnetic fields Impact [108] modified to include hydrodynamic ion motion — showed that the although B-fields initially suppressed the heat-flow, the Nernst effect would eventually displace the magnetic fields from the laser heated region, leading to a delocalization of the electrons and increased heat-flow.

This is illustrated in Fig. 7, which shows the radial profiles of the radial heat-flow and magnetic field for the interaction of an azimuthally symmetric laser beam with a gas-jet under the influence of an externally applied B-field after 440 ps of laser heating. The plot on the left shows that the heat flow is not only suppressed by a 12 T as compared to a 2 T applied field, but with a 12 T field the results of the Vlasov–Fokker–Planck calculation agree with Braginskii theory, implying that nonlocality has been suppressed. The plot on the right shows that the B-field has been completely cavitated from the laser heated region by the Nernst effect for a 2 T applied field. For the 12 T field some advection of the B-field has occurred; given more heating time the laser should completely cavitate the field in this case also, leading to the eventual breakdown of the agreement with Braginskii's transport theory. A convective instability in the Nernst driven flow was also shown to exist by Bissell et al. [118]. Lateral transport of magnetic fields in laser-solid interactions by energetic electrons was also recently demonstrated in 2D Vlasov–Fokker–Planck simulations [119] using a new version of Impact with various modifications, Impacta [120].

Another important effect in the magnetized plasma described by the Vlasov–Fokker–Planck equation is a collisional version of Weibel's instability [121]. Weibel's instability describes a class of self-excited electromagnetic waves arising from anisotropic electron distribution functions in collisionless plasma. The collisional analogue of the instability [122–124], involves the interaction between anisotropic electron pressure and the magnetic field. A very simple picture of what occurs in this instability is as follows: An electron distribution function with anisotropic pressure in the z direction (P_{zz}) can be pictured as an elliptic electron distribution in velocity space with the major axis along z. When a seed magnetic perturbation is applied which varies in x, it will act to rotate the distribution towards the nodes of the magnetic field. This in turn results in a current (from the net flow of electrons coming from both sides of the node) that acts to reinforce the original magnetic perturbation via Ampère's law.

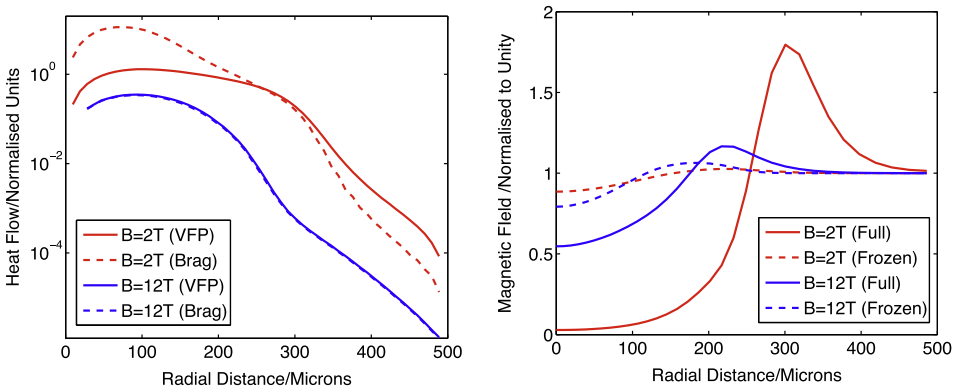

Fig. 7. Ridgers et al.'s calculations of the Nernst effect. Left: radial heat-flow from the laser-heated region under the influence of an externally applied magnetic field after 440 ps, as calculated by the VFP code Impact (solid lines) and as predicted by Braginskii's transport theory (dashed lines). Right: the magnetic field profile from VFP calculations including only frozen-in flow (dashed lines) and with all advection effects — including the Nernst effect (solid lines). *Source:* Reprinted with permission from [114]. Copyright (2008) by the American Physical Society.

The growth-rate for this instability has been calculated by authors using two-fluid calculations [122], but was also studied in some detail in Vlasov–Fokker–Planck calculations by Epperlein [123–125], which improved greatly on the fluid calculations. Epperlein's calculations were also interesting in that he unusually included terms in the expansion of the distribution function up to f_3. This is because the Weibel instability requires f_2 (which describes anisotropic pressure), and f_3 is associated with the heat flux tensor that describes the transport of anisotropic pressure. It turned out to be important in the description because it strongly damps the Weibel growth rate. The amplification of Weibel modes was later studied by Matte et al. [126] in dense plasma. Because of the anisotropy of the oscillation of electrons in the laser field, it was also shown [127–130] that inverse bremsstrahlung heating can lead to Weibel instability. Thomas et al. subsequently simulated this inverse bremsstrahlung driven anisotropic instability [120], using an implicit two-dimensional Vlasov–Fokker–Planck code with magnetic fields and Cartesian tensor expansion to f_2, as in Fig. 8.

5.1. Key algorithm development: methods for implicit differencing of the Vlasov–Fokker–Planck equation

The Vlasov–Fokker–Planck equation may be solved implicitly or explicitly. To illustrate the difference between these approaches consider solving the following 1D partial differential equation:

$$\frac{\partial \alpha}{\partial t} = -\frac{\partial F}{\partial x} \tag{27}$$

Incidentally, this equation describes the flux of α (represented by F) in 1-D. In order to solve this equation numerically its finite difference form must be specified. Consider the way that time is discretized. The left hand side may be approximated by Euler's method:

$$\alpha_i^{n+1} = \alpha_i^n - \Delta t \left(\frac{\partial F}{\partial x}\right)_i^{n*}. \tag{28}$$

The time t^n is defined as that after which n (uniformly spaced) time-steps have occurred, i.e. $t^n = n\Delta t$. The derivative of the flux must be evaluated at the spatial point x_i and at time t^{n*}, where this lies in between times t^n and t^{n+1}. A fully explicit scheme is one where $n*$ is chosen to be the time at which the quantities are known (t^n), a fully implicit scheme is where t^{n*} is the time to which the solution is being advanced (t^{n+1}). Using an explicit scheme imposes a constraint on how large the time-step can be. Information cannot cross more than a single cell in one time-step, if this occurs the numerical solution is unstable and will produce unphysical results — the Courant–Friedrichs–Lewy condition [97]. An implicit scheme on the other-hand is unconditionally stable, although not necessarily accurate. For example, consider a simple thermal diffusion problem; large time steps can be used to obtain the correct global equilibrium solution (i.e. uniform temperature), but the calculated decay rate may be erroneous. Typically an implicit scheme is only first order accurate in time. However, for an appropriately close to equilibrium physical situation, the ability of implicit schemes to take larger time steps can be advantageous for long-time simulations such as inertial confinement fusion scenarios.

If the spatial derivative in Eq. (28) is evaluated by centre-differencing and the time discretization is implicit, then the following equation is arrived at:

$$\alpha_i^{n+1} + \frac{\Delta t}{2\Delta x}\left(F_{i+1}^{n+1} - F_{i-1}^{n+1}\right) = \alpha_i^n. \tag{29}$$

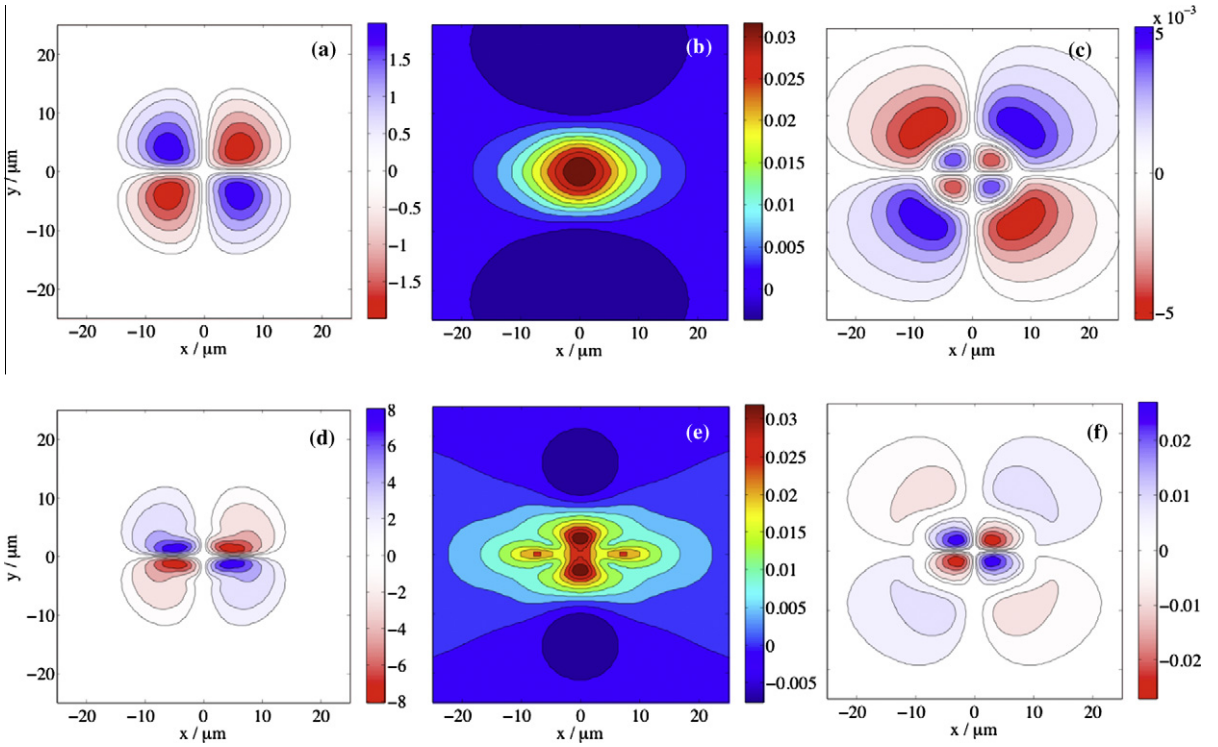

Fig. 8. Calculations of magnetic field generation by anisotropic pressure using IMPACTA in an initially spatially uniform CH plasma with $n_e = 1 \times 10^{20}$ cm^{-3}, average atomic number $\overline{Z} = 5.3$, and atomic mass number $A = 6.5$ heated by a 5 μm diameter laser speckle with $I\lambda^2 = 1 \times 10^{15}$ W cm^{-2} and horizontal polarization. (a–c) Magnetic field in Tesla, $\Delta\Pi/p_e$ and Π_{xy}/p_e after 2.2 ps heating. (d–f) Magnetic field in Tesla, $\Delta\Pi/p_e$ and Π_{xy}/p_e after 4.4 ps heating. *Source:* Reproduced from [120].

The spatial grid-cell size is Δx. In general F is a function of α. Therefore a matrix can be formed for equations like (29) for all the cells in the system. The linear system in this case will be in the form of a tridiagonal matrix as F and so α are required at x_{i-1}, x_i and x_{i+1} in Eq. (29). If the partial differential equation to be solved were more complicated than (27), then the matrix would take a more intricate form. Eq. (29) is then solved by inverting the matrix.

Formulating an implicit differencing scheme is usually relatively straightforward; the key development is the actual numerical solution. One issue with the Maxwell–Vlasov–Fokker–Planck equations is that we frequently encounter nonlinear terms, which are problematic for an implicit solve. One approach is to use a Picard iteration technique [131], which we illustrate using this example of a nonlinear diffusion equation.

$$\frac{\partial \alpha}{\partial t} = \frac{\partial}{\partial x}\left[D(\alpha)\frac{\partial \alpha}{\partial x}\right]. \tag{30}$$

Here α is a generic physical quantity and D is an arbitrary function of α. Treating this equation implicitly yields:

$$\alpha_i^{n+1} = \alpha_i^n + \Delta t\left[\frac{\partial}{\partial x}\left(D\frac{\partial \alpha}{\partial x}\right)\right]_i^{n+1}. \tag{31}$$

This presents a problem, since both of the unknowns D^{n+1} and α^{n+1} cannot be solved for simultaneously. In this case D may be treated as a non-linear coefficient, i.e.:

$$\alpha_i^{n+1,l+1} = \alpha_i^n + \Delta t\left[\frac{\partial}{\partial x}\left(D^{n+1,l}\frac{\partial \alpha^{n+1,l+1}}{\partial x}\right)\right]_i, \tag{32}$$

where $D^{n+1,l}$ is initially D^n. Eq. (32) may then be solved for $\alpha^{n+1,l+1}$. This can then be used to calculate $D^{n+1,l+1}$, which is then reinserted into Eq. (32) as $D^{n+1,l}$ and the solution is computed again. This procedure is iterated until the difference in $\alpha^{n+1,l+1}$ between two iterations $\|\alpha^{n+1,l+1} - \alpha^{n+1,l}\|$ is below a specified tolerance ϵ.

5.2. The development of implicit VFP codes

The 2D Vlasov–Fokker–Planck code SPARK [49] was developed by Epperlein, Rickard and Bell in 1988, using the diffusive approximation. Hydrodynamic ion response was included in 2D as was inverse bremsstrahlung laser absorption [93]. The Vlasov–Fokker–Planck equation was solved implicitly to allow the authors to study long time-scale effects. Note that the code was not *fully* implicit; an 'Alternating Direction Implicit' (ADI) method was used [132]. Under this scheme the spatial derivatives are treated fully implicitly and the velocity derivatives fully explicitly for one time step, this is then switched for the next time-step. The code did not include the effects of magnetic fields.

An early fully implicit code was developed by Mousseau and Knoll [133], which solved the Vlasov–Fokker–Planck equation in one dimension *fully* implicitly, using a Newton–Krylov solver. The first 2D implicit Vlasov–Fokker–Planck code to include magnetic fields self-consistently was IMPACT [108]. Here, the effects of electron–electron collisions were neglected in the $\mathbf{f}_1$ equation and those of electron–ion collisions were neglected in the f_0 equation. The ions were treated as a static neutralising background and inverse bremsstrahlung laser heating was modeled using Langdon's operator [93]. The equations were solved on a 2D Cartesian spatial grid and the magnetic field was constrained to always be perpendicular to this plane (this code was designed to study transport across the B-field). The code used a fully implicit solve for linear terms, with a Picard iteration for nonlinear terms and the magnetic field differenced explicitly. Magnetic fields were included fully implicitly in a later version of the code [120].

To obtain an accurate solution the electron–ion collision time of the thermal electrons (or the shortest time-scale of the phenomena of interest) should be resolved. Long-pulse experiments relevant to inertial confinement fusion have time-scales of the order of a few nanoseconds. The problem with using purely explicit differencing to model such experiments is that they require a time-step which is too small. This can be seen by noting that in any distribution function there will always be a small number of fast particles in the tail moving rapidly. The Courant–Friedrichs–Lewy condition then limits the time-step of an explicit code to be less than the transit time for a grid-cell — this is generally much smaller than an electron–ion collision time (and very much smaller than 1 ns). Additionally, a fully implicit treatment of the electric field increases the robustness of the code and ensures that the rate of change of the magnetic field is stable.

5.3. Field solver methods for Vlasov codes

The correct solution of the Vlasov–Fokker–Planck–Maxwell Eqs. (6)–(8) naturally permit plasma waves, which requires temporal resolution of the plasma period. In some applications, it is also necessary to resolve the plasma period because important physical processes (such as wave–plasma interactions) occur on this timescale; an example would be relativistically-intense laser–plasma interactions. In this case, a standard electromagnetic field solver on, for example, a Yee lattice method [134] can be used. However, for the majority of Vlasov–Fokker–Planck applications — in particular the long time scales of inertial confinement fusion — resolution of the plasma period would make the calculation prohibitively computationally expensive and an implicit method or other means of obtaining the fields is required.

One important field solver approach is the implicit-moment-method outlined in [135], which is stable for $\omega_p \Delta t > 1$. This was originally designed for particle-in-cell simulation, but is easily adapted to the finite-difference Vlasov method. The approach requires predicting the forward-in-time currents by solving the first-order *moment* equation (which gives the temporal evolution of the current density) rather than computing a full implicit timestep forward involving all particles (or velocity grid cells for a Vlasov code). This results in an equation of the form:

$$\frac{\partial \mathbf{j}_s}{\partial t} = -\frac{q_s}{m_s}\nabla \cdot \underline{\underline{P}}_s + \frac{q_s}{m_s}(n_s q_s \mathbf{E} + \mathbf{j}_s \times \mathbf{B}), \tag{33}$$

where $\mathbf{j}_s$ is the current density of species s alone, and the other quantities follow. The forward currents calculated from this equation are then used in a finite difference version of Ampére–Maxwell's Eq. (7):

$$\mathbf{E}^{n+1} = \mathbf{E}^n - \frac{1}{\epsilon_0}\sum_s \mathbf{j}_s^{n^\star}\Delta t + c^2 \nabla \times \mathbf{B}^{n^\dagger}\Delta t, \tag{34}$$

where $n^\star$ and $n^\dagger$ can be varied between n and $n+1$ to choose between stability and accuracy ($\sim n + 1/2$), and absolute stability ($n+1$), to obtain the updated electric field. This is then used in a finite difference version of Faraday's law (Eq. 8) to compute the updated magnetic field. The presence of a magnetic field term in the moment equations complicates the solution if an implicit Lorentz term is required, and sparse-matrix inversion is necessary. Typically a corrective step on the electric field is needed to ensure that quasi-neutrality is maintained over many timesteps [135,136]. This is because the current density from Eq. (33) will yield a *predicted* particle density at $n+1$ which will not be identical to the actual particle density after the predicted fields are used to push particles. Since there is no explicit reference to Gauss's law, $\nabla \cdot \mathbf{E} = \sum_s q_s n_s$, in the equation set, electrons and ions are free to drift from each other and violate quasineutrality. The corrective step calculates an additional electric field contribution corresponding to the difference between the true density and the density consistent with Gauss's law.

Hybrid approaches, that is to say assuming the kinetic particles exist in a background of plasma described by classical transport equations, simplify the matter considerably. By assuming an Ohm's Law is valid [137] in a fluid background, the electric field can be found directly from the fast particle current, $\mathbf{j}_f$, via $\mathbf{E} = -\eta\mathbf{j}_f$ and assuming the fast current is exactly balanced by a cold return current arising as a consequence. Here, η is the resistivity of the fluid background.

In the codes Impact [108] and Impacta [120], a different approach is taken. The easiest case to describe is that of Impacta, which is fully implicit (in Impact the magnetic field is explicitly solved). The equation set includes finite difference versions of the Vlasov–Fokker–Planck equation (expanded in terms of Cartesian tensors), Ampére–Maxwell's and Faraday's equations. The complete equation set is solved fully implicitly using a sparse matrix solver, which means that electric and magnetic fields are calculated that are consistent with the particle density and current density moments. In particular, the matrix contains the finite difference current moment:

$$\mathbf{j}_{i,j} = -e\frac{4\pi}{3}\sum_{k=1}^{n_v}(\mathbf{f}_1)_{i,j,k}v_k^3\Delta v_k, \tag{35}$$

in the Ampére–Maxwell equation. Provided the numerical divergence of the curl of $\mathbf{B}$ is zero, which is ensured by center differencing in space on a simple uniform grid, Ampére–Maxwell is exactly equivalent to Gauss's law for the fully implicit scheme. This can be seen by taking the divergence of Eq. (34) $\nabla\cdot\mathbf{E}^{n+1} = \nabla\cdot\mathbf{E}^n - \nabla\cdot\mathbf{j}^{n+1}\Delta t/\epsilon_0$. Since the continuity equation will be $\rho^{n+1} = \rho^n - \nabla\cdot\mathbf{j}^{n+1}\Delta t$, provided that $\nabla\cdot\mathbf{E}^0 = \rho^0/\epsilon_0$ at $t = 0$, Gauss's law will be obeyed for all time. The difference with respect to the scheme of Mason [135] is the lack of a predictive step, at the expense of a large matrix inversion.

6. Hot electron transport and fast ignition

In 1994, Tabak et al. [12] proposed a new two-stage inertial confinement fusion concept that would later be termed *fast ignition*. The first stage (compression) consists of compressing deuterium–tritium fuel mixture to high density without producing a central hot spot, and the second stage (heating) consists of a very high intensity laser pulse producing a beam of hot (or *fast*) electrons which would propagate up to the highest densities before collisionally depositing their energy. The fast ignition concept provides a route to achieving high gain, and also a reduction in the requirements for compression, which

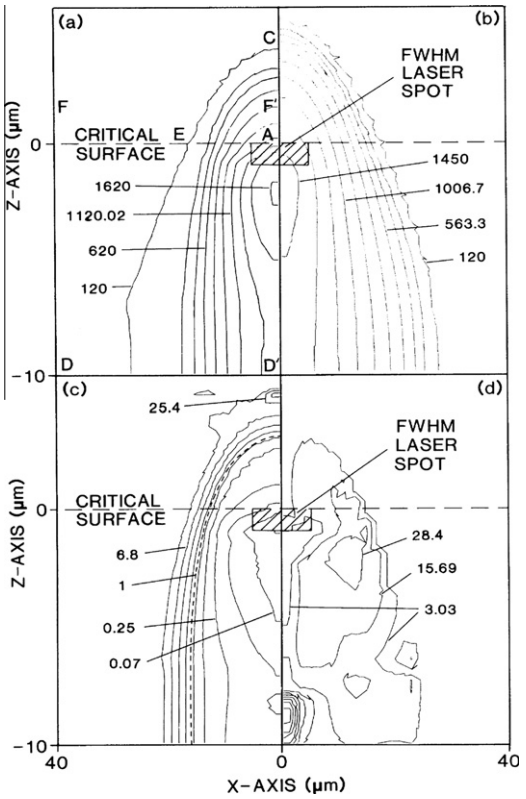

Fig. 9. Two dimensional heat transport calculations using Spark. Contours at 6 ps for a 10 μm laser spot size of (a) temperature in eV from the Fokker–Planck code (contour interval 166.67 eV), (b) temperature in eV from the Spitzer–Härm code (contour interval 147.78 eV), (c) $|\mathbf{q}|/|\mathbf{q}_{Sp}|$, and (d) the angle θ between $\mathbf{q}$ and ∇T_e. *Source:* Reprinted with permission from [147]. Copyright (1989) by the American Physical Society.

means that the total laser energy required for ignition and gain may not exceed a few hundred kJ. The appeal of the fast ignition concept motivated a great deal of both experimental and theoretical research into fast electron generation and transport in the interaction of ultra-intense short pulses with overdense plasmas. This was greatly helped by the investment in short-pulse ultra-intense laser facilities around the world in the 1990s and 2000s. For fast ignition, one needs electrons of a few MeV in order to produce the required hot spot, a requirement set by the collisional range in deuterium–tritium fuel [138]. The typical temperature of the fast electron population at a given intensity is thought to lie fairly close to the scaling provided by Wilks [139], $T_{fast} \approx 0.511\left(\sqrt{1+(I\lambda^2)/(1.38\times10^{18}\ \mathrm{W\,cm^{-2}\,\mu m^2})}-1\right)$ MeV.

From this scaling, intensities on the order of 10^{19}–10^{20} W cm^{-2} and wavelengths of 300–1000 nm are sufficient to produce the required mean electron energy. Although these electrons will be stopped quickly at the highest ($\rho > 300$ g cm^{-3}) densities, around solid densities these electrons have collision periods on the order of several ps. Therefore a substantial part of the fast electron propagation from the point of generation to the compressed core will have low collisionality. The fast electron beam will have a very high current density, exceeding 10^{16} A m^{-2}. The return current from cold background plasma that will evolve to locally cancel the fast current density will be highly collisional. Thus a resistively generated electric field will be set up. This electric field will have a significant curl, sufficient to generate magnetic fields exceeding 100 T during the laser pulse duration. This can potentially lead to magnetic collimation of the fast electron beam, but the same physics also makes strong filamentation of the beam a possibility. The magnetic field generation critically depends on the plasma resistivity, which may not be accurately given by the classical Spitzer–Härm resistivity either.

The modeling of fast electron transport therefore ideally requires a fully kinetic simulation model [140] with proper treatment of all collisions. This is highly computationally demanding, and a number of different approaches have been followed as a result; a hybrid fluid particle-in-cell model, [137,141], a collisional particle-in-cell model [142–145], expanded Vlasov–Fokker–Planck treatment [96], and a full/hybrid Vlasov–Fokker–Planck model [146].

6.1. Vlasov–Fokker–Planck codes for fast electron transport

Vlasov–Fokker–Planck codes have made a significant contribution to the study of fast electron transport. An early first attempt at modeling a short pulse interaction (in this case a 3.5 ps laser) was performed by Rickard et al. [147] in 2D with hydrodynamic ions using the Spark code [49], looking at the comparison of the heat flow calculated with the code with the Spitzer–Härm [71] heat flow $\mathbf{q}_{SH} = -\kappa\nabla T_e$ from laser heating from a finite focal spot. This is also significant in being an early example of 2D Vlasov–Fokker–Planck simulation. The heat flux, laser absorption and other characteristics of ultrashort laser plasma interactions was also later studied by Drska et al. [148,149].

Fig. 9 shows contour plots of the 2D heat transport calculations carried out by Rickard et al., showing (a) temperature in eV from the Fokker–Planck code, (b) temperature in eV from the Spitzer–Härm code, (c) the ratio of heat flux to the Spitzer–Härm heat flux, $|\mathbf{q}|/|\mathbf{q}_{Sp}|$, and (d) the angle θ between $\mathbf{q}$ and ∇T_e. These show a number of interesting features. In particular, both the magnitude (c) and the direction (d) of the heat flux are shown to depart dramatically from the Spitzer–Härm heat flux. For small laser spots, lateral heat transport is suppressed, meaning that heat transport into the target is not strongly reduced [147].

For a short pulse interaction, ionization dynamics can be very important as this can proceed on a timescale comparable to the laser pulse-length. Marchand and Matte [150] proposed a simple algorithm for solving the Vlasov–Fokker–Planck equation using the Chang–Cooper scheme [43] with terms representing the collisional ionization processes included in the finite difference integrals of the collision operator. This model was later improved by Town et al. [117,151] to include three-body recombination.

One of the most predominant uses of Vlasov–Fokker–Planck codes in modeling short-pulse interactions has been to study the basic physics of fast electron transport, for example Bell's study of resistive magnetic field generation and subsequent collimation of the fast electron beam [152] (Fig. 10), the work by Sherlock on non-Spitzer return currents [153], and investigations by Robinson and Sherlock on artificially induced beam collimation [154,155] all using the Kalos algorithm. Other notable results from Vlasov–Fokker–Planck codes include studies of electron thermal transport [156], the effects of magnetic fields on core heating in fast ignition [157], heating and ionization in solid targets [158,159], and a return current instability [160].

The Kalos method, which was pioneered by Bell et al. [152], uses a spherical harmonic decomposition of the distribution function, including relativistic distributions, and allows for an arbitrary number of terms to be kept in the expansion in order to describe the system with sufficient accuracy. This enables modeling of highly anisotropic distributions that develop when intense short laser pulses are incident on overdense plasmas.

Solving these equations with an explicit method implies that the time-step must be such as to resolve plasma waves, which can be a significant limitation in this scheme, especially for solid density plasmas ($n_e = 10^{23}$ cm^{-3} or more). For such plasmas the Courant–Friedrichs–Lewy condition restricts the time-step to $\omega_p\,\Delta t \lesssim 1 \Rightarrow \Delta t \lesssim 0.056$ fs, so that for a 1 ps-long simulation about 2×10^5 time-steps are required. Moreover, because the distribution function can include many harmonics the simulation demands large amount of memory and the total amount of computation required can be very large. Nevertheless, the rapid progress and increasing availability of high performance computing resources have made such simulations possible.

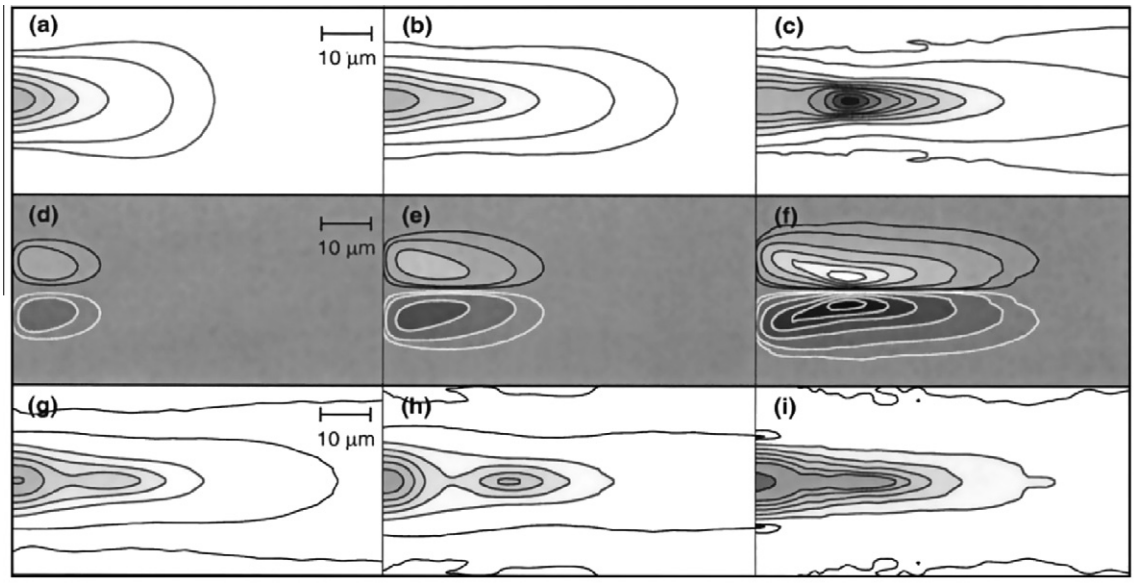

Fig. 10. Resistive collimation of fast electrons. Spatial plots (close to the axis) of temperature (a)–(c) and (g)–(i) for various parameters. (d)–(f), respectively, plot the magnetic field for cases (a)–(c). The temperature contour levels are 350, 400, 600, 800, 1000, 1200, 1400, 1800, 2200, and 2600 eV. The magnetic field contour levels are ±0.1, 0.2, 0.5, 1.0, 1.5, and 2.0 MG. *Source:* Reprinted with permission from [152]. Copyright (2003) by the American Physical Society.

In 1D calculations it is possible to use a very high number of harmonics, and thus model extremely anisotropic distributions, and even laser absorption [161]. Studies of fast electron transport using Vlasov–Fokker–Planck codes have modelled the fast electron generation in terms of an energy deposition process in a similar fashion to hybrid codes. Recently the Kalos formalism was implemented in the Oshun code [55], where it was demonstrated that physics of highly anisotropic relativistic distributions, such as the relativistic two-stream and current filamentation instabilities, can be simulated using Vlasov–Fokker–Planck codes in multiple dimensions in configuration-space.

Another notable implementation, the Fido code developed by Sherlock [146,162], is an Eulerian-gridded Vlasov solver with momentum space grid in spherical polar coordinates (i.e. $f(x,y,|p|,\theta,\phi)$, not an expansion in spherical harmonics) with the full Fokker–Planck operator included in the code. The Eulerian approach allows simulations in regimes where the advective terms in the Vlasov–Fokker–Planck equation are dominant, for example acceleration in strong electric fields. This was recently used to examine the expansion of two dimensional sheaths on the rear of solid targets to infer the angular divergence of a fast-electron beam [163], and also the coupling of relativistic electron beams with hydrodynamic ion motion in the solid target [164].

6.2. Extended particle-in-cell modeling for inertial confinement fusion

The particle-in-cell method [165–168] in its basic form statistically represents the Vlasov equation through the use of a series of discrete charge clouds, which exist in a 6*N*-dimensional phase space analogous to the original Liouville system of classical point particles. The principal difference between the particle-in-cell method and a standard particle method such as molecular dynamics [169] is that the interactions between particles are mediated by fields calculated on a finite-differenced grid, but importantly *the particles are still allowed to occupy an arbitrary location in position space*. This circumvents having to compute the huge number of binary interactions between individual particles while retaining *N*-body phenomena.

The mediation of the grid enables efficient simulations of large systems, but it also introduces some complications. The non-conservative force associated with the particle-grid mapping leads to self-heating and in some cases to numerical instability, and modifies the plasma properties. Nevertheless, if the resolution is high enough, such that $\Delta x \ll \lambda_D$, the effects associated with the aliasing terms are unimportant. Traditional particle-in-cell simulations resolve λ_D, and have been shown to be an excellent and versatile tool for modeling plasmas in many different regimes.

In typical inertial confinement fusion plasmas the density and temperature span a vast range of parameters. This includes regions where the density/temperature is high/low enough that the Debye length is on the order of few Angstroms. Simulating these regions using particle-in-cell codes with $\Delta x < \lambda_D$ is not practical. On the other hand, near the critical density, where the Debye length is long, the ability of particle-in-cell codes to sample the phase-space and to self-consistently model the complex absorption processes and plasma instabilities is unparalleled.

When the Debye length is small, the number of particles in a Debye sphere $N_D = (4\pi/3)n\lambda_D^3$ is also small and collisions become more significant. In this regime plasma waves are heavily damped and low-frequency long-wavelength phenomena are usually of interest. The latter can be captured with a particle-in-cell code, without resolving λ_D, provided that there are

enough particles to ensure their collisionality is negligible. Collisions must then be taken into account separately using a Monte-Carlo collision operator. Under these conditions, collisional particle-in-cell simulations employing high-order splines and coarse resolution can be used to study the physics of inertial confinement fusion plasmas.

Shanny et al. [170] first proposed a Monte-Carlo technique for performing large angle binary collisions between particles, equivalent to a series of cumulative small angle scatterings [71,171], and showed it to be equivalent to the Fokker–Planck operator for a large enough number of particles. Takizuka and Abe [143] later extended this to a multi-component plasma and developed a robust algorithm for dealing with collisions. In their paper, the key computational step is to pair particles within a cell randomly and perform a rotation in the center-of-mass frame, which conserves both total momentum and energy. Only performing collisions between pairs reduces the $\sim N^2$ potential interactions to $\sim N$ calculations. The rotation angle is calculated from $\tan(\theta/2)$, using the collision frequency in Eq. (1) multiplied by the time step Δt, from the variance $\langle \tan^2(\theta/2)\rangle = \nu_{1,2}\Delta t$, with a Gaussian probability distribution. This method has been discussed by other authors, particularly with respect to the choice of collision frequency [144,172,173], and generalized for relativistic particles, relevant to fast ignition, by Sentoku et al. [174,145].

More recently, Peano et al. [175] have shown that for relativistic particles this method does not relax to the correct (Jüttner) distribution, and proposed an alternative Monte-Carlo method. These collision operators differ from those typically used in Vlasov–Fokker–Planck codes and this difference is indicative of the fundamental differences between particle-in-cell and Vlasov–Fokker–Planck approaches. Such a model has been used for studies of cone-guided fast ignition [176] and the collisional relaxation of suprathermal electrons [177]. Using a "particle-moment method" collision operator [178], the VPIC particle-in-cell code has been used to study Raman and Brillouin scattering instabilities in the hohraum gas fill using petascale computing [179].

6.3. Hybrid particle–fluid modeling

In a hybrid particle-in-cell code [137,141,180], the background plasma is treated as a fluid with a prescribed resistivity as a function of the background temperature. The electric field is determined by a simple Ohm's Law, and Maxwell's equations are thus reduced to an induction equation. The background plasma evolves according to fluid equations, and heats due to both Ohmic heating (resistive return current) and the collisional drag on the fast electrons. Fast electrons are treated fully kinetically via a particle-in-cell or a Vlasov fluid distribution.

To extend the applicability of the particle approach to ultra-high density plasmas, thereby allowing for the physics of the plasma corona to be seamlessly coupled to the physics of the dense core, a new hybrid algorithm was recently developed by Cohen [181]. This scheme uses the particle-in-cell description for particles throughout the simulation domain, but above certain density, $n \sim 100 n_c$, Ohm's law is employed to prescribe the electric field associated with the background plasma. This method effectively boosts the performance of the collisional particle-in-cell method — otherwise severely constrained by its massive computational requirements — to enable integrated modeling of experiments. For dealing with collisions in the hybrid scheme, a model was developed by Sherlock [182] to implement Coulomb collisions in a fluid plasma background by reducing the Fokker–Planck equation into a Langevin form.

7. The National Ignition Facility to the present

Point design for the National Ignition Facility has required an extensive simulation campaign in support of preparations for experiments. Vlasov–Fokker–Planck simulations are currently too intensive to allow full scale simulation of a National Ignition Facility implosion, and so hydrodynamic simulation has been utilized [11]. However, since kinetic simulations provide a more accurate physical model in certain situations, they can be used to benchmark methods included in hydrodynamic codes to attempt to replicate kinetic effects — flux limiters for example. The kinetic models can be used to model and comprehend instabilities in small regions of parameter space, in the hope that the understanding gained will lead to improvements in large scale simulations. Hence, the nonlocal heat transport problem in particular is still being extensively studied to the present day using Vlasov–Fokker–Planck codes [89,183,184,94].

One important advance on previous investigations was the extension of codes to two dimensions. Epperlein et al. developed a two dimensional Vlasov–Fokker–Planck code, SPARK [116,117], and used it to demonstrate the ineffectiveness of nonlocal electron transport in smoothing temperature inhomogeneities on scale-lengths smaller than $\sim$100 electron mean-free-paths [49]. The lasers used as implosion drivers will have their intensity profiles randomly distributed in a series of hot spots, or speckles of high intensity, by the use of random phase plates [185]. The speckle pattern has a coherence time of less than the hydrodynamic time-scale (1–10 ps), so that in principle the ion fluid experiences a relatively uniform heating profile [186]. It is therefore important to study the smoothing of temperature inhomogeneities. This problem has also been studied in different contexts by other authors [187,188].

Sunahara and coworkers [189] used a Legendre expanded Vlasov–Fokker–Planck code for electrons, including terms to f_3, coupled to a fluid code LILAC in one spatial dimension to study electron thermal conduction. The results were not only compared to a Spitzer–Härm fluid code, but also to experiment (Fig. 11) through neutron production rates from data obtained using the OMEGA laser system. These show good agreement, but with the Spitzer–Härm code requiring a time varying flux limiter. Another demonstration of kinetic effects in experiment was the use of IMPACT [108] to help interpret the Thomson

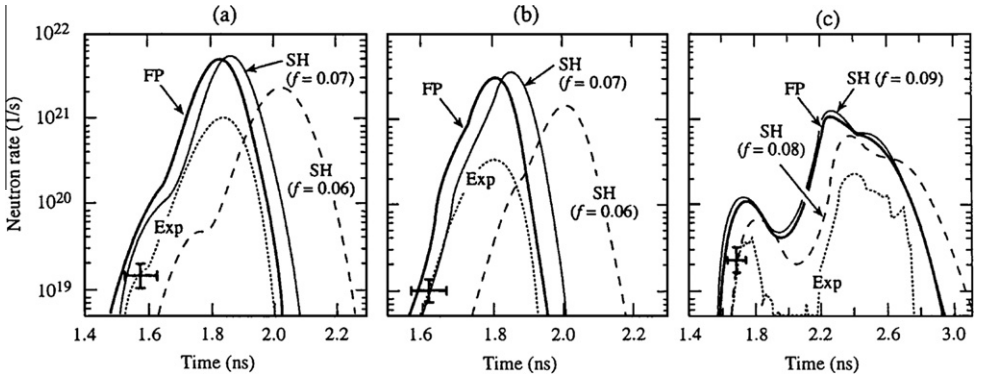

Fig. 11. Sunahara et al. simulate Omega experiments. Comparison of neutron rates calculated by Fokker–Planck and Spitzer–Härm of $f = 0.07$ and 0.06. (a) 15 atm of D_2 fuel gas and 1 ns square pulse, (b) 3 atm of D_2 fuel gas and 1 ns square pulse, and (c) 20 atm of DT fuel and 0. 4 ns square pulse. *Source:* Reprinted with permission from [189]. Copyright (2003) by the American Physical Society.

scattering spectrum in planar ablating plasma between the critical and ablation surfaces. Asymmetry in the peaks in the spectrum were much better described by a dynamic form factor $S(k,\omega)$ using a distribution function from the Vlasov–Fokker–Planck code compared with a classical transport calculation. As a result, this was inferred to be the first measurement of a non-classical electron distribution function in this scenario [190].

Bell [66] also studied the effect of electron energy transport on ion acoustic waves, which were also studied by Afeyan et al. [191] in the context of parametric instabilities. A somewhat related problem of ion density perturbation smoothing was recently examined by Keskinen [192] with an expanded two dimensional Vlasov–Fokker–Planck code using the diffusive approximation. In this case, the ions were also kinetically modeled using a similar diffusive approximation Vlasov–Fokker–Planck description to the electrons [193]. Keskinen found that initial ion density perturbations could be smoothed on hydrodynamic timescales, and that the kinetic model gave more smoothing than a Spitzer–Härm model (Fig. 12).

Keskinen also showed that radiation transport may also be important in determining the electron transport properties with a Vlasov–Fokker–Planck code coupled to a radiation hydrodynamics code [194]. Other authors have used Vlasov–Fokker–Planck simulation techniques to study nonlocal heat transport in comparison to the results from hydrodynamic codes [195,196]. Brantov et al. [197] studied the propagation of nonlocal heat waves using a Fokker–Planck simulation, showing good agreement with an analytic model that was developed. Another issue is the actual fusion process itself in the compressed core. Fokker–Planck methods have also recently been used in calculations of the effects of details in the ion distribution function during deuterium–tritium fusion reactions [198,199].

7.1. Shock ignition

Another recent development is the shock ignition approach to inertial confinement fusion [13,200,201], which involves cryogenic shells imploded with a low implosion velocity, leading to fuel assemblies with large areal densities. Subsequently, the assembled fuel is ignited from a central hot spot heated by the collision of a spherically convergent ignitor shock and also the returning original shock, leading to a hot spot pressure exceeding that of the surrounding dense fuel. The ignitor shock is generated by a correctly timed spike in the pulse power. Thermonuclear gain can be significantly larger than in conventional

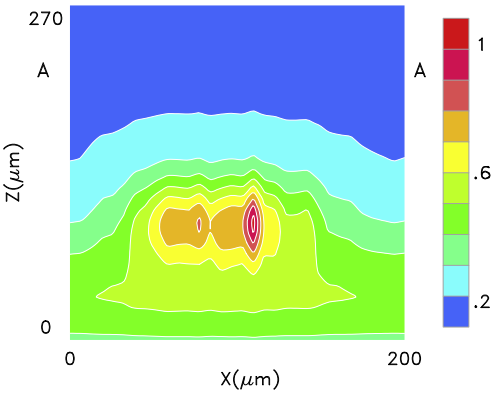

Fig. 12. Thermal smoothing in nonuniform laser targets. Plot of 2D variation of Fokker–Planck electron temperature T_e vs. x and z at $t = 420$ ps. Temperature has been normalized to 2.2 keV. The symbol A denotes the position of the ablation surface. *Source:* Reprinted with permission from [192]. Copyright (2009) by the American Physical Society.

Table 2
Qualitative summary of the benefits and drawbacks of different approaches to simulating ICF plasma.

Aspect	PIC (collisionless)	PIC (binary collisions)	PIC (hybrid)	VFP (full)	VFP (hybrid)	VFP (expanded)	Fluid
Efficiency	High	High	High	Low	Reasonable	Reasonable	High
Time/space constraint	Restrictive (fs, 10 μm)	Restrictive (fs, 10 μm)	Somewhat restrictive (ps, 100 μm)	Restrictive (fs, μm)	Somewhat restrictive (ps, 100 μm)	Reasonable (ps, 100 μm – ns, mm)	Good (full scale simulation)
Noise/finesse	Poor	Poor	Fair	Good	Good	Good	Good
Treatment of collisionless phenomena	Good	Good	Good	Good	Good	Good–Poor (depends on no. expansion terms)	Limited
Treatment of semi-collisional phenomena ($\ln \Lambda_{ei} \gg 1$)	None	Good	None	Good	Good	Good	None
Treatment of highly-collisional phenomena ($\ln \Lambda_{ei} \leqslant 1$)	None	None	Reasonable	None	Reasonable	None	Reasonable

isobaric ignition for equal driver energy, as a lower energy threshold for ignition is required. Essentially, in this scheme the assembly of the dense fuel (compression) and volumetric heating due to the *PdV* work of the high-velocity shock are decoupled — the same motivation as that for fast ignition.

Although this is a rather recent development in inertial confinement fusion research, some modeling has been performed both hydrodynamically [202] and kinetically using particle-in-cell simulation [203]. However, full particle-in-cell simulation is restricted by the requirement to resolve the plasma period and in the latter studies the time-scale was restricted to less than a few 10 s of picoseconds. In particular, a complete unknown is parametric instabilities and hot electron generation during the spike–plasma interaction in the corona [204], as well as strong magnetic field generation and its effect on the symmetry of the shock propagation. Ion shocks were previously modeled under fusion related conditions using a Vlasov–Fokker–Planck code by Casanova et al. [205], who showed that ion viscosity and thermal conduction effects were much larger than hydrodynamic simulations would suggest. Kinetic effects in ion transport were subsequently been simulated using Vlasov–Fokker–Planck methods by a number of authors [206–208].

More recently, 1D Vlasov–Fokker–Planck simulations of electron transport in shock-ignition-relevant scenarios were compared with hydrodynamic models by Bell and Tzoufras [209]. In this work it was argued that nonlocal transport can facilitate the production of more effective shocks, thus suggesting that shock ignition designs in which the laser intensity exceeds 10^{15} W cm^{-2} can lead to lower ignition threshold and higher gain. Work in this area is ongoing.

8. Conclusions

Vlasov–Fokker–Planck numerical simulation techniques for inertial confinement fusion research have been extensively used and studied for 30 years, enabling a large number of important physics discoveries that have helped us understand the nature of such interactions. The field is fertile, with a number of new numerical techniques emerging recently. The different techniques all have their strengths, weaknesses and applicability to various regions of the overall interaction.

8.1. A comparison of the different numerical techniques

Simulating an inertial confinement fusion plasma is extremely difficult for the reasons we have outlined in this review. In attempting to do so, researchers have employed a number of models, from calculations using the multiphysics fluid code Lasnex [11] to study full scale simulations of the implosion, to the studies of regions of the interaction described in this review using kinetic simulation techniques. It is useful to briefly review the various merits of each technique, fluid, finite difference Vlasov–Fokker–Planck and finite particle methods. These are summarized in Table 2. Particle-in-cell (PIC) methods are listed with the headings Collisionless, Binary collisions, and Hybrid methods; Vlasov–Fokker–Planck (VFP) methods are listed as Full, Hybrid and Expanded, with Full being the full finite-differenced phase-space, Hybrid [146] having the same basic fluid model as the PIC Hybrid model, and Expanded meaning using the spherical harmonic or Cartesian tensor expansion.

The first three aspects of the codes, ''Efficiency'', ''Time/space constraint'' and ''Noise/finesse'' are rather qualitative. Efficiency is how the information is stored, it relates to how fast a typical code is expected to be, and is the most subjective rating. Fluid and particle-in-cell methods store information in a minimal way, and are therefore both listed as ''High'', despite the fact that clearly a fluid code lacks information on the phase space. Full Vlasov–Fokker–Planck would typically contain the most redundancy of information storage, as the full phase space needs to be stored. Hybrid and Expanded Vlasov–Fokker–Planck are listed as ''Reasonable'' as they store momentum phase-space information in a more efficient way than Full Vlasov–Fokker–Planck. Time/space constraint is also somewhat subjective, and is based on running a ''typical'' code on a ''typical'' cluster of ~100 processors in terms of what are the maximum length and timescales that could be ''reasonably

simulated" for a hot solid target interaction, based on the timescales in published results. Noise/finesse entries are more quantitative, in that Vlasov–Fokker–Planck and fluid codes are naturally smooth, whereas particle-in-cell methods are subject to noise due to the finite number of discrete particles, with the Hybrid particle-in-cell being essentially a δf-method, and therefore naturally being less subject to noise [210,211]. It is worth making the point that while particle-in-cell codes tend to be noisy, which in some cases may provide an unreasonably large seed perturbation for instabilities to grow from, Vlasov–Fokker–Planck codes may be unrealistically smooth. It is possible that numerical diffusion in Vlasov–Fokker–Planck codes damps real physical instabilities.

The last three aspects describe the relative treatment of phenomena in different regimes of $\ln\Lambda_{ei}$ and the relative evaluations are therefore purely due to the physical equations involved. The reason that fluid codes are listed as having "limited" ability to model collisionless phenomena is that for some collisionless phenomena such as electron plasma waves a fluid description is adequate, but for phenomena such as wavebreaking, a fluid description breaks down. Similarly, the reason a fluid code is listed as having no treatment of semicollisional phenomena is because this refers to physics where the velocity dependence of the collision operator, and therefore the details of the shape of the distribution function, is important. An example of this is nonlocal transport, which cannot be correctly described with a fluid model without the addition of some other operator, in the absence of being able to solve the infinite chain of moment equations.

The most profound difference between particle codes and Vlasov type codes is the issue of graininess, with particle codes exhibiting artificially high levels of it and Vlasov codes completely lacking it. The presence of granularity in particle-in-cell codes is not fundamentally an issue of inadequate statistics, because no matter how high the number of simulation particles is, graininess will never completely disappear from a particle-in-cell code (as is also true for an actual physical system). This allows particle-in-cell codes to model instabilities from noise and to incorporate physics associated with complex particle trajectories. For inertial confinement fusion plasmas however, the lack of statistical smoothness can obscure and modify the physics. Furthermore, numerical effects associated with finite size simulation particles can severely compromise the reliability of the results.

Vlasov and Vlasov–Fokker–Planck codes produce results without noise, which allow for clear physical pictures to emerge. Single modes can be isolated and studied individually and since Vlasov–Fokker–Planck codes represent the plasma using distribution functions, lack of statistics is never an issue. However, if the distribution function is not described with sufficient detail the physics cannot be modelled accurately, and as a result Vlasov–Fokker–Planck codes are also prone to numerical artifacts. Vlasov–Fokker–Planck codes also miss the microphysics of individual particles, and N-body interactions. For inertial confinement fusion plasmas these effects can be especially pronounced near the critical surface, but deep in the target, where the distribution function is quickly isotropized due to collisions, Vlasov–Fokker–Planck codes can be very efficient and they provide high fidelity modeling of the physics.

Another crucial difference between the two methods, relating to numerics, is that while particle codes sample the phase-space to provide a sparse but extensive representation of it, Vlasov–Fokker–Planck codes use distribution functions to model a smaller area with much higher detail. This has important consequences in how the codes are used. Near the laser–plasma interaction region, where the plasma has a very wide range of temperatures, but where the λ_D is large, particle-in-cell codes are ideal. Deep in the plasma, where the distribution function is close to a Gaussian, the temperatures are low and the λ_D is small, Vlasov–Fokker–Planck codes can be used much more efficiently.

8.2. Current status and recent developments in Vlasov–Fokker–Planck simulation

Algorithmic development in Vlasov–Fokker–Planck research is ongoing, with many recent innovations in code evolution and progress. Recent methods include a numerical procedure that puts the equation in a form amenable to parabolic partial differential equation methods [212], a model involving an angular closure M_1 expansion leading to hyperbolic equations [213] and a completely conservative form of the Landau version of the Fokker–Planck operator [214]. Another interesting development that has been recently demonstrated is a direct finite difference Cartesian Maxwell–Fokker–Planck–Landau code employing fast algorithms [215].

For short pulse modeling, the spherical harmonic based Kalos algorithm has recently been extended to multiple dimensions including a semi-anisotropic collision operator [55]. Nevertheless, the Kalos algorithm is not the only Vlasov–Fokker–Planck approach being pursued. A 2D2P Eulerian Vlasov solver has very recently been developed by Sircombe and co-workers (Valis [216]), and has recently been augmented with a Bhatnagar–Gross–Krook collision operator [80] to approximate collisional behavior fully implicitly [217]. The algorithms that have been developed for Eulerian Vlasov solvers in a Cartesian phase space are robust, and this has been amply demonstrated by the ability of these codes to model the laser interaction. On the other hand, such codes do require a considerable amount of memory for useful calculations. Other recent Vlasov–Fokker–Planck codes developed for fast electron transport relevant to fast ignition include a code similar to Epperlein's model [218], a relativistic Fokker–Planck code named RFP-2D [219,220], which has also been coupled to a hydrodynamic bulk plasma model [221].

The interaction of intense, nanosecond laser pulses with plasma has been the subject of intense international study over the last three decades, culminating in the recent successful completion of the National Ignition Facility and the soon to be completed Laser MegaJoule in France. The leading motivation for this has been the realization of inertial confinement fusion schemes for both energy production and as part of the stockpile stewardship program. The development of intense short-pulse lasers producing high-current fluxes of extremely high-energy electrons has transformed the inertial fusion energy

field by introducing the possibility of achieving ignition and gain through fast ignition. Numerical simulation of the kinetics of hot electrons and ions is extremely computationally demanding, and there is no single code that can capture all relevant aspects whilst making few approximations and requiring modest computational resources. Although Vlasov–Fokker–Planck codes are not the most widely used computational model, they have made a valuable contribution to this line of research both in terms of providing an alternative model to benchmark against experimental and fluid-code results, and in particular because of the physics insights that they have provided in their own right.

Acknowledgments

AGRT would like to thank Ed Larsen for useful discussions and the University of Michigan for financial support. M.T., A.R.B., C.P.R. and R.J.K. would like to acknowledge the HiPER laser project for financial assistance.

Appendix A. The Cartesian tensor expansion

A.1. Expansion of f using Cartesian tensors

Here we show explicitly how to expand the Vlasov equation componentwise in terms of Cartesian tensors. First we can identify five terms in the Vlasov–Fokker–Planck equation:

$$\text{(i)}\ \frac{\partial f}{\partial t} + \text{(ii)}\ \mathbf{p}\cdot\nabla f + \text{(iii)}\ q\mathbf{E}\cdot\frac{\partial f}{\partial \mathbf{p}} + \text{(iv)}\ q\mathbf{p}\times\mathbf{B}\cdot\frac{\partial f}{\partial \mathbf{p}} = \text{(v)}\ \left(\frac{\delta f}{\delta t}\right)_c. \tag{36}$$

These terms can be expanded in terms of direction cosines $\cos\theta_{x_i}$ following a similar method to Ref. [86], where $\theta_{x_i} \equiv \{\theta_x, \theta_y, \theta_z\}$, as follows:)

(i)

$$\frac{\partial f}{\partial t} = \frac{\partial f_0}{\partial t} + \sum_{l,x_1,\ldots x_l} \frac{\partial}{\partial t} f_{l,x_1,\ldots x_l} \prod_{t=1}^{l} \cos\theta_{x_t}. \tag{37}$$

(ii)

$$\mathbf{v}\cdot\nabla f = |v| \cos\theta_{x_i} \left[\frac{\partial f_0}{\partial r_i} + \sum_{l,x_1,\ldots x_l} \frac{\partial}{\partial r_i} f_{l,x_1,\ldots x_l} \prod_{t=1}^{l} \cos\theta_{x_t}\right]. \tag{38}$$

(iii)

$$\mathbf{E}\cdot\frac{\partial f}{\partial \mathbf{p}} = \frac{E_i}{\cos\theta_{x_i}} \frac{\partial f_0}{\partial p} + \sum_{l,x_1,\ldots x_l} \frac{f_{l,x_1,\ldots x_l}}{p} \sum_{s=1}^{l} E_{x_s} \frac{1}{\cos\theta_{x_s}} \prod_{t=1}^{l} \cos\theta_{x_t} + \sum_{l,x_1,\ldots x_l} p^l E_i \cos\theta_{x_i} \left(\prod_{t=1}^{l} \cos\theta_{x_t}\right) \frac{\partial}{\partial p}\left[\frac{f_{l,x_1,\ldots x_l}}{p^l}\right]. \tag{39}$$

(iv)

$$\mathbf{v}\times\mathbf{B}\cdot\frac{\partial f}{\partial \mathbf{p}} = \sum_{l,x_1,\ldots x_l} f_{l,x_1,\ldots x_l} \sum_{s=1}^{l} \frac{\epsilon_{x_s ij} B_j \cos\theta_{x_i}}{\cos\theta_{x_s}} \prod_{t=1}^{l} \cos\theta_{x_t}. \tag{40}$$

(v) The collision terms are rather more complicated, and unlike the other four terms will depend on what particular species we are describing (electrons or ions).

A.2. The coupled chain of Cartesian tensor angular moment equations

By explicitly taking the angular moments and simplifying, a coupled chain of equations results for each of the components of the distribution function f_m. These represent an evolution equation for each f_m in terms of itself, and neighboring terms, f_{m+1} and f_{m-1}. The first four orders of these equations are:

$m = 0$

$$4\pi\left[\frac{\partial f_0}{\partial t} + \frac{|v|}{3}\frac{\partial f_{1i}}{\partial r_i} + \frac{qE_i}{3p^2}\frac{\partial}{\partial p}\left(p^2 f_{1i}\right) = C_0\right], \tag{41}$$

$m = 1$

$$\frac{4\pi}{3}\left[\frac{\partial f_{1i}}{\partial t} + |v|\frac{\partial f_0}{\partial r_i} + \frac{2}{5}|v|\frac{\partial f_{2ij}}{\partial r_j} + qE_i\frac{\partial f_0}{\partial p} + \frac{2}{5p^3}qE_j\frac{\partial}{\partial p}\left(p^3 f_{2ij}\right) + \epsilon_{ijk}qB_j f_{1k} = C_{1i}\right], \tag{42}$$

m

$$\frac{8\pi}{15}\left[\frac{\partial f_{2ij}}{\partial t}+\frac{|v|}{2}\left(\frac{\partial f_{1i}}{\partial r_j}+\frac{\partial f_{1j}}{\partial r_i}\right)-\frac{|v|}{3}\frac{\partial f_{1k}}{\partial r_k}\delta_{ij}+\frac{p}{2}\frac{\partial}{\partial p}\left\{\frac{1}{p}\left(qE_i f_{1j}+qE_j f_{1i}-\frac{2}{3}\delta_{ij}f_{1k}qE_k\right)\right\}\right.$$
$$\left.+\frac{3}{7}\left[p\frac{\partial}{\partial r_k}+qE_k\frac{1}{p^4}\frac{\partial}{\partial p}p^4\right]f_{3ijk}+qB_k(\epsilon_{ikn}f_{2jn}+\epsilon_{jkn}f_{2in})=C_{2ij}\right], \tag{43}$$

$m = 3$

$$\frac{8\pi}{35}\left[\frac{\partial f_{3ijk}}{\partial t}-\frac{2|v|}{15}\frac{\partial}{\partial r_n}\left(f_{2in}\delta_{jk}+f_{2jn}\delta_{ik}+f_{2kn}\delta_{ij}\right)+\frac{|v|}{3}\left(\frac{\partial f_{2jk}}{\partial r_i}+\frac{\partial f_{2ik}}{\partial r_j}+\frac{\partial f_{2ij}}{\partial r_k}\right)-\frac{2qE_n}{15}p^2\frac{\partial}{\partial p}\frac{1}{p^2}\left(f_{2in}\delta_{jk}+f_{2jn}\delta_{ik}+f_{2kn}\delta_{ij}\right)\right.$$
$$+\frac{p^2}{3}\frac{\partial}{\partial p}\frac{1}{p^2}\left(qE_i f_{2jk}+qE_j f_{2ik}+qE_k f_{2ij}\right)+B_n\epsilon_{qpn}\left(f_{3iqp}\delta_{jk}+f_{3jqp}\delta_{ik}+f_{3kqp}\delta_{ij}\right)+B_n\left(\epsilon_{inq}f_{3qjk}+\epsilon_{jnq}f_{3qik}+\epsilon_{knq}f_{3qij}\right)$$
$$\left.+\mathsf{T}_{ijk}\left(f_{4x_1x_2x_3x_4}\right)=C_{3ijk}\right]. \tag{44}$$

A.3. Components of the direction cosine moments of the Vlasov–Fokker–Planck equation

The Fokker–Planck collision terms, $C_{la_1\ldots a_l}$, are the sum of contributions of like-particle (e.g. electron–electron) and unlike-particle (e.g. electron–ion) collision terms [24]. For like-particles, taking angular moments of the Fokker–Planck operator yields:

$$C_0=\frac{Y}{3p^2}\frac{\partial}{\partial p}\left(A_0 f_0+B_0\frac{\partial f_0}{\partial p}\right). \tag{45}$$

For higher order terms, the terms become increasingly complicated. For simplicity, here we only consider electron collisions with other particles (either other electrons or ions). In the limit that $p_e \gg p_{ion}$ with a sufficiently close to Maxwellian ion momentum distribution, the first few order collision terms are given by:

$$C_{1i}=\frac{Y}{3p^2}\left[-\frac{A_0(f_{\text{ions}})}{p}f_{1i}+\frac{\partial}{\partial p}\left(A_0 f_{1i}+B_0\frac{\partial f_{1i}}{\partial p}\right)-\left(\frac{\partial B_0}{\partial p}+A_0\right)f_{1i}+\frac{p}{5}\left(3\{B_1\}_i\frac{\partial^2 f_0}{\partial p^2}-\frac{\partial}{\partial p}\{B_1\}_i\frac{\partial f_0}{\partial p}\right)+\frac{\{A_1\}_i}{3}\frac{\partial f_0}{\partial p}+12\pi f_0 f_{1i}p^2\right]$$
$$+\mathcal{O}(m_e/m_{\text{ion}}), \tag{46}$$

$$C_{2ij}=-\frac{A_0(f_{\text{ions}})}{p^3}f_{2ij}+\{C_{2ee}\}_{ij}+\mathcal{O}(m_e/m_{\text{ion}}) \tag{47}$$

$$C_{3ijk}=-\frac{6A_0(f_{\text{ions}})}{p^3}f_{3ijk}+\{C_{3ee}\}_{ijk}+\mathcal{O}(m_e/m_{\text{ion}}) \tag{48}$$

where:

$$A_i=3I^i_i;\quad B_i=\left(I^i_{2+i}+J^i_{-1-i}\right), \tag{49}$$

$$I^i_j=\frac{4\pi}{p^j}\int_0^p f_i u^{j+2}du;\quad J^i_j=\frac{4\pi}{p^j}\int_p^\infty f_i u^{j+2}du, \tag{50}$$

$$Y=4\pi\left(\frac{ZZ'e^2}{4\pi\epsilon_0 m_e}\right)^2\ln\Lambda_{ei} \tag{51}$$

and Z and Z' are the charge number for the colliding particle and its target respectively. Note that here i is a component index and *ion* indicates quantities relating to ions. The electron–ion collision operators can be simplified, under the assumption that the ions are cold so that their thermal velocity spread is much less than the electron velocity, to reduce to:

$$C_m=-\frac{m(m+1)Y}{p^3}f_m. \tag{52}$$

A.4. Cosine integral relations

The time evolution of the various components of f can be found by taking the moments m of the Vlasov–Fokker–Planck equation in momentum unit vectors $\{\hat{\mathbf{p}}\}^m$:

$$\int d\Omega\{\hat{\mathbf{p}}\}^m\left[\frac{\partial f}{\partial t}+\mathbf{p}\cdot\nabla f+q\mathbf{E}\cdot\frac{\partial f}{\partial\mathbf{p}}+q\mathbf{p}\times\mathbf{B}\cdot\frac{\partial f}{\partial\mathbf{p}}=\left(\frac{\delta f}{\delta t}\right)_c\right]. \tag{53}$$

This integral can be performed component-wise in terms of the direction cosines over 4π solid angle Ω. For example, the spatial derivative component of the Vlasov–Fokker–Planck equation for the $m = 2$ moment would be:

$$|v|\frac{\partial}{\partial r_k}\int_{4\pi}\cos\theta_i\cos\theta_j\cos\theta_k\left(f_0+f_{1a_1}\cos\theta_{a1}+f_{2a_1a_2}\cos\theta_{a1}\cos\theta_{a2}+\cdots\right)d\Omega. \tag{54}$$

To calculate the moments of the Vlasov–Fokker–Planck equation in terms of direction cosines, the following integral relations can be used:

$$\int_{4\pi} d\Omega = 4\pi; \quad \int_{4\pi}\cos\theta_i\,d\Omega = 0,$$
$$\int_{4\pi}\cos\theta_i\cos\theta_j d\Omega = \frac{4\pi}{3}\delta_{ij}; \qquad \int_{4\pi}\cos\theta_i\cos\theta_j\cos\theta_k\,d\Omega = 0,$$
$$\int_{4\pi}\cos\theta_i\cos\theta_j\cos\theta_k\cos\theta_l d\Omega = \frac{4\pi}{15}\left(\delta_{ij}\delta_{kl}+\delta_{ik}\delta_{jl}+\delta_{il}\delta_{jk}\right),$$
$$\int_{4\pi}\cos\theta_i\cos\theta_j\cos\theta_k\cos\theta_l\cos\theta_m\,d\Omega = 0.$$

$$\int_{4\pi}\cos\theta_i\cos\theta_j\cos\theta_k\cos\theta_l\cos\theta_m\ cos\theta_n d\Omega = \frac{4\pi}{105}\left\{\begin{array}{l}\delta_{ij}(\delta_{kl}\delta_{mn}+\delta_{km}\delta_{ln}+\delta_{kn}\delta_{lm})\\ +\delta_{ik}\left(\delta_{jl}\delta_{mn}+\delta_{jm}\delta_{ln}+\delta_{jn}\delta_{lm}\right)\\ +\delta_{il}\left(\delta_{jk}\delta_{mn}+\delta_{jm}\delta_{kn}+\delta_{jn}\delta_{km}\right)\\ +\delta_{im}\left(\delta_{jk}\delta_{ln}+\delta_{jl}\delta_{kn}+\delta_{jn}\delta_{kl}\right)\\ +\delta_{in}\left(\delta_{jk}\delta_{lm}+\delta_{jl}\delta_{km}+\delta_{jm}\delta_{kl}\right)\end{array}\right\},$$

where δ_{mn} is the Kronecker delta, which takes the value 1 for $m = n$ and 0 otherwise, and ϵ_{ijk} is the Levi-Cevita operator, which takes the value 1 for even permutations of i, j and k, -1 for odd permutations and 0 otherwise.

References

[1] J.D. Lindl, Inertial Connement Fusion, Springer, New York, 1998.
[2] S. Atzeni, J. Meyer-ter Vehn, The Physics of Inertial Fusion, Oxford University Press, Oxford, 2004.
[3] E.I. Moses, in: 36th IEEE International Conference on Plasma Science, San Diego, CA, May 31–June 05, 2009, IEEE Trans. Plasma Sci. 38 (4, Part 2 Sp. Iss. SI) (2010) 684.
[4] J.D. Lindl, E.I. Moses, Phys. Plasmas 18 (5) (2011).
[5] J. Lindl, Phys. Plasmas 2 (11) (1995) 3933.
[6] J. Lindl et al, Phys. Plasmas 11 (2) (2004) 339.
[7] S.H. Glenzer et al, Phys. Rev. Lett. 106 (8) (2011) 085004.
[8] A.A. Vlasov, Zh. Eksp. Teor. Fi. 8 (3) (1957) 291.
[9] A.A. Vlasov, Sov. Phys. Uspekhi – USSR 10 (6) (1968) 721.
[10] R.E. Olson et al, in: Sixth International Conference on Inertial Fusion Sciences and Applications, Parts 1–4, San Francisco, CA, September 06–11, 2009, Journal of Physics Conference Series, vol. 244, IOP Publishing Ltd., England, 2010, p. 032057.
[11] G. Zimmerman et al, J. Opt. Soc. Am. 68 (4) (1978) 549.
[12] M. Tabak et al, in: 35th Annual Meeting of the Division-of-Plasma-Physics of the American-Physical-Society, St. Louis, Mo, November 01–05, 1993, Phys. Plasmas 1 (5, Part 2) (1994) 1626.
[13] R. Betti et al, Phys. Rev. Lett. 98 (15) (2007) 155001.
[14] A.R. Bell, R.G. Evans, D.J. Nicholas, Phys. Rev. Lett. 46 (4) (1981) 243.
[15] J. Nuckolls et al, Nature 239 (5368) (1972) 139.
[16] T.j. Gilmartin et al, IEEE J. Quant. Electron. 11 (9) (1975) D32.
[17] Rayleigh, Proc. London Math. Soc. s1–14 (1) (1882) 170.
[18] G. Taylor, Proc. Roy. Soc. London Ser. A – Math. Phys. Sci. 201 (1065) (1950) 192.
[19] T. Gilmartin, J. Opt. Soc. Am. 68 (4) (1978) 548.
[20] S.L. Kahalas et al, J. Fusion Energy 10 (1991) 93, doi:10.1007/BF01306864.
[21] K. Mima et al, in: 17th Topical Meeting on the Technology of Fusion Energy, Madison, WI, September 14–16, 2004, Fusion Sci. Technol. 47 (3) (2005) 662.
[22] P. Debye, E. Hückel, Physik. Zeits. 24 (1923) 185.
[23] E. Rutherford, Phylos. Mag. 21 (1911) 669.
[24] I.P. Shkarofsky, T.W. Johnston, M.P. Bachynski, The Particle Kinetics of Plasmas, Addison-Wesley, Reading, Massachusetts, 1966.
[25] A.D. Fokker, Ann. Phys. Berlin 43 (5) (1914) 810.
[26] M. Planck, Sitzber. K. Preuss. Akad. Wiss. 1 (1917) 324.
[27] S. Chandrasekhar, Rev. Mod. Phys. 15 (1) (1943) 0001.
[28] M.N. Rosenbluth, W.M. MacDonald, D.L. Judd, Phys. Rev. 107 (1) (1957) 1.
[29] C.-K. Li, R.D. Petrasso, Phys. Rev. Lett. 70 (20) (1993) 3063.
[30] S. Atzeni, Plasma Phys. Controlled Fusion 51 (12) (2009) 124029.
[31] B.J. Braams, C.F.F. Karney, Phys. Rev. Lett. 59 (16) (1987) 1817.
[32] L.D. Landau, Phys. Z. Sowjetunion 10 (1936) 154.
[33] A.A. Arsenev, O.E. Buryak, Math. USSR-Sbornik 69 (2) (1991) 465.
[34] W.M. MacDonald, M.N. Rosenbluth, W. Chuck, Phys. Rev. 107 (2) (1957) 350.
[35] J. Killeen, A.H. Futch, J. Comput. Phys. 2 (3) (1968) 236.
[36] G.F. Bing, J.E. Roberts, Phys. Fluids 4 (8) (1961) 1039.
[37] H. Dreicer, Phys. Rev. 117 (2) (1960) 343.
[38] L.L. House, P.N. Swartztrauber, Phys. Fluids 10 (3) (1967) 605.
[39] D. Montgomery, L. Turner, G. Joyce, Phys. Fluids 17 (5) (1974) 954.

[40] J.C. Whitney, J. Comput. Phys. 6 (3) (1970) 483.
[41] R.S. Cohen, L. Spitzer, P.M. Routly, Phys. Rev. 80 (2) (1950) 230.
[42] I.P. Shkarofsky, Can. J. Phys. 41 (11) (1963) 1753.
[43] J.S. Chang, G. Cooper, J. Comput. Phys. 6 (1) (1970) 1.
[44] E. Larsen et al, J. Comput. Phys. 61 (3) (1985) 359.
[45] C. Buet, S. Dellacherie, Commun. Math. Sci. 8 (4) (2010) 1079.
[46] A.V. Bobylev, V.A. Chuyanov, USSR Comput. Math. Math. Phys. 16 (2) (1976) 121.
[47] A. Langdon, in: CECAM Workshop Proceedings, 1981.
[48] T.H. Kho, Phys. Rev. A 32 (1) (1985) 666.
[49] E.M. Epperlein, G.J. Rickard, A.R. Bell, Phys. Rev. Lett. 61 (21) (1988) 2453.
[50] E.M. Epperlein, J. Comput. Phys. 112 (2) (1994) 291.
[51] P. Degond, B. Lucquin-Desreux, Numer. Math. 68 (2) (1994) 239.
[52] C. Buet et al, J. Comput. Phys. 133 (2) (1997) 310.
[53] M. Lemou, L. Mieussens, C.R. Math. 338 (10) (2004) 809.
[54] F. Alouani-Bibi, M.M. Shoucri, J.P. Matte, in: 18th International Conference on the Numerical Simulation of Plasmas, Falmouth, MA, September 07–10, 2003, Comput. Phys. Commun. 164 (1–3) (2004) 60.
[55] M. Tzoufras et al, J. Comput. Phys. 230 (17) (2011) 6475.
[56] L. Chacon et al, J. Comput. Phys. 157 (2) (2000) 618.
[57] L. Chacon et al, J. Comput. Phys. 157 (2) (2000) 654.
[58] L. Pareschi, G. Russo, G. Toscani, J. Comput. Phys. 165 (1) (2000) 216.
[59] F. Filbet, L. Pareschi, J. Comput. Phys. 179 (1) (2002) 1.
[60] Z. Xiong et al, J. Comput. Phys. 227 (15) (2008) 7192.
[61] W.R. Briley, H. McDonald, J. Comput. Phys. 34 (1) (1980) 54.
[62] R.C. Malone, R.L. McCrory, R.L. Morse, Phys. Rev. Lett. 34 (12) (1975) 721.
[63] D.R. Gray et al, Phys. Rev. Lett. 39 (20) (1977) 1270.
[64] D. Shvarts et al, Phys. Rev. Lett. 47 (4) (1981) 247.
[65] R.J. Mason, Phys. Rev. Lett. 47 (9) (1981) 652.
[66] A.R. Bell, Phys. Fluids 26 (1) (1983) 279.
[67] D.J. Bond, Phys. Lett. A 88 (3) (1982) 144.
[68] S.A. Khan, T.D. Rognlien, Phys. Fluids 24 (8) (1981) 1442.
[69] J. Albritton, Phys. Rev. Lett. 50 (26) (1983) 2078.
[70] A. Fick, Philos. Mag. S.4 10 (1855) 30.
[71] L. Spitzer, R. Harm, Phys. Rev. 89 (5) (1953) 977.
[72] W.L. Kruer, Comments Plasma Phys. Controlled Fusion 5 (1979) 69.
[73] J.F. Luciani, P. Mora, J. Virmont, Phys. Rev. Lett. 51 (18) (1983) 1664.
[74] P.A. Holstein et al, J. Appl. Phys. 60 (7) (1986).
[75] A. Bendib, J.F. Luciani, J.P. Matte, Phys. Fluids 31 (4) (1988) 711.
[76] E.M. Epperlein, R.W. Short, Phys. Fluids B – Plasma Phys. 3 (11) (1991) 3092.
[77] G.P. Schurtz, P.D. Nicolai, M. Busquet, Phys. Plasmas 7 (10) (2000) 4238.
[78] P. Nicolai, J. Feugeas, G. Schurtz, Phys. Plasmas 13 (3) (2006) 032701.
[79] B. Frolov et al, New J. Phys. 8 (4) (2006) 56.
[80] P. Bhatnagar, E. Gross, M. Krook, Phys. Rev. 94 (3) (1954) 511.
[81] W. Manheimer, D. Colombant, V. Goncharov, Phys. Plasmas 15 (8) (2008) 083103.
[82] D. Colombant, W. Manheimer, Phys. Plasmas 15 (8) (2008) 083104.
[83] D. Colombant, W. Manheimer, Phys. Plasmas 16 (6) (2009) 062705.
[84] D. Colombant, W. Manheimer, J. Comput. Phys. 229 (11) (2010) 4369.
[85] D.G. Colombant, W.M. Manheimer, Phys. Plasmas 17 (11) (2010) 112706.
[86] T.W. Johnston, Phys. Rev. 120 (4) (1960) 1103.
[87] C. Cheng, G. Knorr, J. Comput. Phys. 22 (3) (1976) 330.
[88] J.P. Matte, J. Virmont, Phys. Rev. Lett. 49 (26) (1982) 1936.
[89] A.R. Bell, Phys. Fluids 28 (6) (1985) 2007.
[90] E.M. Epperlein, J. Phys. D – Appl. Phys. 17 (9) (1984) 1823.
[91] S. Braginskii, Rev. Plasma Phys. 1 (1966) 205.
[92] J.P. Matte et al, Phys. Rev. Lett. 53 (15) (1984) 1461.
[93] A.B. Langdon, Phys. Rev. Lett. 44 (9) (1980) 575.
[94] J. Li et al, Plasma Phys. Controlled Fusion 52 (8) (2010) 085008.
[95] B. Ersfeld, A.R. Bell, Phys. Plasmas 7 (3) (2000) 1001.
[96] A. Bell et al, Plasma Phys. Controlled Fusion 48 (3) (2006) R37.
[97] R. Courant, K. Friedrichs, H. Lewy, Math. Ann. 100 (1928) 32.
[98] P. Colella, P.R. Woodward, J. Comput. Phys. 54 (1) (1984) 174.
[99] T. Arber, R. Vann, J. Comput. Phys. 180 (2002).
[100] S.H. Glenzer, W.E. Alley, K.G. Estabrook, J.S. De Groot, M.G. Haines, J.H. Hammer, J.-P. Jadaud, B.J. MacGowan, J.D. Moody, W. Rozmus, L.J. Suter, T.L. Weiland, E.A. Williams, Phys. Plasmas 6 (1999) 2117–2128.
[101] L. Biermann, Z. Naturfors, Sect. A – J. Phys. Sci. 5 (2) (1950) 65.
[102] W.M. Manheimer, D.G. Colombant, J.H. Gardner, Phys. Fluids 25 (9) (1982) 1644.
[103] J.A. Stamper et al, Phys. Rev. Lett. 26 (17) (1971) 1012.
[104] R. Craxton, Phys. Rev. Lett. 35 (20) (1975) 1336.
[105] C.K. Li et al, Phys. Rev. Lett. 102 (20) (2009).
[106] L. Willingale et al, Phys. Plasmas 17 (4) (2010).
[107] R.J. Kingham, A.R. Bell, Phys. Rev. Lett. 88 (4) (2002) 045004.
[108] R.J. Kingham, A.R. Bell, J. Comput. Phys. 194 (1) (2004) 1.
[109] J. Nakarmi, L. Jha, in: H. Sugai, T. Hayashi (Eds.), ICPP 96 Contributed Papers – Proceedings of the 1996 International Conference on Plasma Physics, Nagoya, Japan, September 09–13, vols. 1 and 2, 1997, pp. 1662–1665.
[110] C.P. Ridgers et al, Phys. Plasmas 15 (9) (2008) 092311.
[111] A. Nishiguchi et al, Phys. Rev. Lett. 53 (3) (1984) 262.
[112] T.H. Kho, M.G. Haines, Phys. Rev. Lett. 55 (8) (1985) 825.
[113] J.F. Luciani, P. Mora, A. Bendib, Phys. Rev. Lett. 55 (22) (1985) 2421.
[114] C.P. Ridgers, R.J. Kingham, A.G.R. Thomas, Phys. Rev. Lett. 100 (7) (2008) 075003.
[115] D.H. Froula et al, Phys. Rev. Lett. 98 (13) (2007) 135001.

[116] E.M. Epperlein, G.J. Rickard, A.R. Bell, Comput. Phys. Commun. 52 (1) (1988) 7.
[117] R.P.J. Town, A.R. Bell, S.J. Rose, Phys. Rev. E 50 (2, Part B) (1994) 1413.
[118] J.J. Bissell, C.P. Ridgers, R.J. Kingham, Phys. Rev. Lett. 105 (17) (2010) 175001.
[119] L. Willingale et al, Phys. Rev. Lett. 105 (9) (2010) 095001.
[120] A.G.R. Thomas, R.J. Kingham, C.P. Ridgers, New J. Phys. 11 (2009) 033001.
[121] E.S. Weibel, Phys. Rev. Lett. 2 (3) (1959) 83.
[122] T. Mochizuki et al, Jpn. J. Appl. Phys. 19 (10) (1980).
[123] E. Epperlein, Plasma Phys. Controlled Fusion 27 (9) (1985) 1027.
[124] E. Epperlein, Plasma Phys. Controlled Fusion 28 (1b) (1986) 393.
[125] E.M. Epperlein, A.R. Bell, Plasma Phys. Controlled Fusion 29 (1) (1987) 85.
[126] J.P. Matte, A. Bendib, J.F. Luciani, Phys. Rev. Lett. 58 (20) (1987) 2067.
[127] A.Y. Romanov, V.P. Silin, S.A. Uryupin, JETP 84 (4) (1997) 687.
[128] A. Bendib, K. Bendib, A. Sid, Phys. Rev. E 55 (6) (1997) 7522.
[129] B. Dubroca et al, Phys. Plasmas 11 (8) (2004) 3830.
[130] A. Sangam, J.P. Morreeuw, V.T. Tikhonchuk, Phys. Plasmas 14 (5) (2007) 053111.
[131] E. Picard, J. Math. Pure Appl. 6 (1890) 197.
[132] D.W. Peaceman, H.H. Rachford Jr., J. Soc. Ind. Appl. Math. 3 (1) (1955) 28.
[133] V. Mousseau, D. Knoll, J. Comput. Phys. 136 (2) (1997) 308.
[134] K.S. Yee, IEEE Trans. Antennas Propagat. AP14 (3) (1966) 302.
[135] R.J. Mason, J. Comput. Phys. 71 (2) (1987) 429.
[136] B. Marder, J. Comput. Phys. 68 (1) (1987) 48.
[137] J.R. Davies et al, Phys. Rev. E 56 (6) (1997) 7193.
[138] S. Atzeni, A. Schiavi, C. Bellei, Phys. Plasmas 14 (2007) 052702.
[139] S. Wilks, W. Kruer, IEEE J. Quant. Electron. 33 (1997) 1954.
[140] R.G. Evans, in: 34th European-Physical-Society Conference on Plasma Physics, Warsaw, Poland, July 02–06, 2007, Plasma Phys. Controlled Fusion 49 (12B) (2007) B87.
[141] J.R. Davies, Phys. Rev. E 65 (2002) 026407.
[142] C.K. Birdsall, A.B. Langdon, Plasma Physics via Computer Simulation, Adam Hilger, New York, 1991.
[143] T. Takizuka, H. Abe, J. Comput. Phys. 25 (3) (1977) 205.
[144] K. Nanbu, Phys. Rev. E 55 (4) (1997) 4642.
[145] Y. Sentoku, A. Kemp, J. Comput. Phys. 227 (14) (2008) 6846.
[146] M. Sherlock, Phys. Plasmas 16 (10) (2009) 103101.
[147] G.J. Rickard, A.R. Bell, E.M. Epperlein, Phys. Rev. Lett. 62 (23) (1989) 2687.
[148] L. Drska, J. Limpouch, R. Liska, Laser Part. Beams 10 (3) (1992) 461.
[149] J. Limpouch, L. Drska, R. Liska, Laser Part. Beams 12 (1) (1994) 101.
[150] R. Marchand, J.P. Matte, J. Comput. Phys. 97 (2) (1991) 352.
[151] R.P.J. Town, A.R. Bell, S.J. Rose, Phys. Rev. Lett. 74 (6) (1995) 924.
[152] A. Bell, R. Kingham, Phys. Rev. Lett. 91 (3) (2003) 035003.
[153] M. Sherlock et al, Phys. Plasmas 14 (10) (2007) 102708.
[154] A.P.L. Robinson, M. Sherlock, Phys. Plasmas 14 (8) (2007) 083105.
[155] A.P.L. Robinson, M. Sherlock, P.A. Norreys, Phys. Rev. Lett. 100 (2) (2008) 025002.
[156] M. Honda et al, Phys. Plasmas 3 (9) (1996) 3420.
[157] T. Johzaki, Y. Nakao, K. Mima, Phys. Plasmas 16 (6) (2009) 062706.
[158] J.P. Matte et al, Phys. Rev. Lett. 72 (8) (1994) 1208.
[159] F. Bibi, J. Matte, J. Kieffer, in: Workshop on Simulations of Ultra Intense Laser Beams Interaction with Matter, Bordeaux, France, April 14–16, 2003, Laser Particle Beams 22 (2) (2004) 97.
[160] V.T. Tikhonchuk et al, Phys. Plasmas 2 (11) (1995) 4169.
[161] M. Sherlock, A.R. Bell, W. Rozmus, Laser Particle Beams 24 (2) (2006) 231.
[162] M. Sherlock, Phys. Rev. Lett. 104 (2010) 205004.
[163] C.P. Ridgers et al, Phys. Rev. E 83 (3, Part 1) (2011) 036404.
[164] R.J. Kingham et al., in: Sixth International Conference on Inertial Fusion Sciences and Applications, San Francisco, CA, Sep 06–11, Parts 1–4, Journal of Physics Conference Series, vol. 244, 2010, p. 022042.
[165] O. Buneman, Phys. Rev. 115 (3) (1959) 503.
[166] J. Dawson, Phys. Fluids 5 (4) (1962) 445.
[167] A.B. Langdon, C.K. Birdsall, Phys. Fluids 13 (8) (1970) 2115.
[168] J. Dawson, Rev. Mod. Phys. 55 (2) (1983) 403.
[169] W. Hoover, A. Ladd, V. Hoover, Adv. Chem. Ser. (204) (1983) 29.
[170] R. Shanny, J.M. Dawson, J.M. Greene, Phys. Fluids 10 (6) (1967) 1281.
[171] B.A. Trubniko, Y.N. Yavlinsk, Sov. Phys. JETP 21 (6) (1965) 1088.
[172] A.V. Bobylev, K. Nanbu, Phys. Rev. E 61 (4) (2000) 4576.
[173] C. Wang et al, J. Comput. Phys. 227 (9) (2008) 4308.
[174] Y. Sentoku, A. Kemp, T. Cowan, in: 4th International Conference on Inertial Fusion Sciences and Applications, Biarritz, France, September 04–09, 2005, J. Phys. IV 133 (2006) 425.
[175] F. Peano et al, Phys. Rev. E 79 (2) (2009) 025701.
[176] B. Chrisman, Y. Sentoku, A.J. Kemp, in: 49th Annual Meeting of the Division of Plasma Physics of the American-Physical-Society, Orlando, FL, November 12–16, 2007, Phys. Plasmas 15 (5) (2008) 056309.
[177] A.J. Kemp et al, Phys. Rev. Lett. 97 (23) (2006) 235001.
[178] D.S. Lemons et al, J. Comput. Phys. 228 (5) (2009) 1391.
[179] L. Yin et al, Phys. Rev. Lett. 99 (26) (2007).
[180] L. Gremillet, G. Bonnaud, F. Amiranoff, Phys. Plasmas 9 (3) (2002) 941.
[181] B.I. Cohen, A.J. Kemp, L. Divol, J. Comput. Phys. 229 (12) (2010) 4591.
[182] M. Sherlock, J. Comput. Phys. 227 (4) (2008) 2286.
[183] J.M. Liu et al, Phys. Plasmas 1 (11) (1994) 3570.
[184] A.V. Brantov et al, Phys. Plasmas 5 (7) (1998) 2742.
[185] Y. Kato et al, Phys. Rev. Lett. 53 (11) (1984) 1057.
[186] I. Voronich, Quant. Electron. 31 (11) (2001) 970.
[187] S. Brunner, E. Valeo, Phys. Plasmas 9 (3) (2002) 923.
[188] J.-L. Feugeas et al, Phys. Plasmas 15 (6) (2008) 062701.
[189] A. Sunahara et al, Phys. Rev. Lett. 91 (9) (2003) 095003.

[190] J. Hawreliak et al, J. Phys. B – At. Mol. Opt. Phys. 37 (7) (2004) 1541.
[191] B.B. Afeyan et al, Phys. Rev. Lett. 80 (11) (1998) 2322.
[192] M.J. Keskinen, Phys. Rev. Lett. 103 (5) (2009) 055001.
[193] M.J. Keskinen, Phys. Plasmas 17 (5) (2010) 054507.
[194] M.J. Keskinen, A. Schmitt, in: International Conference on Interaction of Atoms, Molecules and Plasmas with Intense Ultrashort Laser Pulses, Szeged, Hungary, October 01–05, 2006, Laser Particle Beams 25 (3) (2007) 333.
[195] Q.Z. Yu et al, Phys. Plasmas 17 (4) (2010) 043106.
[196] D. Ya-Lin, Z. Bin, Z. Jian, Chinese Phys. 16 (12) (2007) 3742.
[197] A. Brantov et al, in: 18th International Conference on the Numerical Simulation of Plasmas, Falmouth, MA, September 07–10, 2003, Comput. Phys. Commun. 164 (1–3) (2004) 67.
[198] M. Sherlock, S.J. Rose, A.P.L. Robinson, Phys. Rev. Lett. 99 (25) (2007) 255003.
[199] M. Sherlock, S.J. Rose, High Energy Density Phys. 5 (1-2) (2009) 27.
[200] X. Ribeyre et al, in: 10th International Workshop on Fast Ignition of Fusion Targets, Crete, Greece, June 09–18, 2008, Plasma Phys. Controlled Fusion 51 (1) (2009) 015013.
[201] L.J. Perkins et al, Phys. Rev. Lett. 103 (4) (2009) 045004.
[202] M. Lafon, X. Ribeyre, G. Schurtz, Phys. Plasmas 17 (5) (2010) 052704.
[203] O. Klimo et al, Plasma Phys. Controlled Fusion 52 (5) (2010) 055013.
[204] B. Canaud, M. Temporal, New J. Phys. 12 (2010) 043037.
[205] M. Casanova, O. Larroche, J.P. Matte, Phys. Rev. Lett. 67 (16) (1991) 2143.
[206] F. Vidal et al, Phys. Fluids B – Plasma Phys. 5 (9) (1993) 3182.
[207] F. Vidal et al, Phys. Rev. E 52 (4, Part B) (1995) 4568.
[208] O. Larroche, Eur. Phys. J. D 27 (2) (2003) 131.
[209] A.R. Bell, M. Tzoufras, Plasma Phys. Controlled Fusion 53 (4) (2011) 045010.
[210] J. Koga, T. Tajima, J. Comput. Phys. 116 (2) (1995) 314.
[211] R. Sydora, J. Comput. Appl. Math. 109 (1–2) (1999) 243.
[212] S. Wollman, E. Ozizmir, J. Comput. Phys. 228 (18) (2009) 6629.
[213] B. Dubroca, J.L. Feugeas, M. Frank, Eur. Phys. J. D 60 (2) (2010) 301.
[214] I.F. Potapenko, C.A. de Azevedo, J. Comput. Appl. Math. 103 (1) (1999).
[215] R. Duclous et al, J. Comput. Phys. 228 (14) (2009) 5072.
[216] N. Sircombe, J. Comput. Phys. 104 (2010) 205004.
[217] T.D. Arber, N.J. Sircombe, in: Sixth International Conference on Inertial Fusion Sciences and Applications, Parts 1–4, San Francisco, CA, Sep 06–11, 2009, Journal of Physics Conference Series, vol. 244, IOP Publishing Ltd., England, 2010, p. 022017.
[218] Z. Bin, Z. Jian, Plasma Sci. Technol. 10 (1) (2008) 22.
[219] T. Yokota et al, Laser Phys. 16 (7) (2006) 1111.
[220] T. Yokota et al, Phys. Plasmas 13 (2) (2006) 022702.
[221] T. Yokota et al, in: 4th International Conference on Inertial Fusion Sciences and Applications, Biarritz, France, September 04–09, 2005, J. Phys. IV 133 (2006) 433.